



Predicting Human Upper Extremity Reaching Motions: Comparison of Optimization-Based Method and Heuristic Method

Estela Pérez Luque, Seunghun Lee, Dan Högberg, James Yang & Maurice Lamb

To cite this article: Estela Pérez Luque, Seunghun Lee, Dan Högberg, James Yang & Maurice Lamb (16 Mar 2026): Predicting Human Upper Extremity Reaching Motions: Comparison of Optimization-Based Method and Heuristic Method, International Journal of Human-Computer Interaction, DOI: [10.1080/10447318.2026.2632154](https://doi.org/10.1080/10447318.2026.2632154)

To link to this article: <https://doi.org/10.1080/10447318.2026.2632154>



© 2026 The Author(s). Published with license by Taylor & Francis Group, LLC



Published online: 16 Mar 2026.



Submit your article to this journal [↗](#)



View related articles [↗](#)



View Crossmark data [↗](#)

Predicting Human Upper Extremity Reaching Motions: Comparison of Optimization-Based Method and Heuristic Method

Estela Pérez Luque^a , Seunghun Lee^b , Dan Högberg^a , James Yang^b  and Maurice Lamb^c 

^aSchool of Engineering Science, University of Skövde, Skövde, Sweden; ^bDepartment of Mechanical Engineering, Texas Tech University, Lubbock, TX, USA; ^cSchool of Informatics, University of Skövde, Skövde, Sweden

ABSTRACT

Predicting human upper extremity reaching motion in 3D space can support adaptive interactions with computer-controlled systems (robots and virtual avatars), and applications in ergonomics and rehabilitation. This study compares two predictive approaches: an optimization-based method (OPM) and a proposed heuristic method (SFM) that integrates steering dynamics path planning, an adaptive velocity model, and inverse kinematics. Both methods were validated against motion capture data from ten participants performing four reach tasks. Predictions and inter-subject variability were evaluated for path, velocity, and upper extremity joint configuration using root mean square error and dynamic time warping. Results show that SFM more accurately predicts spatial path and velocity, whereas OPM achieves greater precision in joint angle estimation. As input, OPM requires the initial and end postures and the task duration, while SFM needs the initial posture, initial and target end-effector positions, and initial and estimated peak velocity. These results highlight trade-offs between accuracy and behavioral variability when selecting motion prediction methods.

KEYWORDS

Human motion prediction; optimization; heuristic; time series; dynamic time warping

1. Introduction

Predictive human motion methods have long been an interest of researchers from a variety of disciplines (Gang & Wang, 2025). The ability to model and predict human movements without relying on recorded motion data enables advancements in a wide range of applications, including ergonomics, digital human modeling (DHM), virtual reality, animation, robotics, and particularly human–computer interaction, where accurate and adaptive motion prediction can enhance interaction with computer-controlled systems such as robots and digital human models (Demirel et al., 2022).

Within human–computer interaction, DHM emerged as a field for simulating human–system interactions and supporting design evaluations through digital manikins. However, despite its potential, DHM still faces challenges regarding realism and fidelity of posture and motion prediction (Demirel et al., 2022; Perez Luque et al., 2022). These challenges motivate the development of new or complementary approaches for motion prediction that can provide more accurate representations of human movement in 3D spaces.

Among the many types of actions that humans perform, reaching motions are one of the most frequently performed types of goal-directed action in daily life (Furuiki & Takiyama, 2017). Accurately predicting reaching motions requires capturing both the spatial and temporal dynamics of movement throughout the reaching arm, from the path of the hand (i.e., end-effector) through the angles of each joint in the upper extremity (e.g., wrist, elbow, and shoulder) for the duration of a reach motion. When evaluating observed and predicted reaching motions, three interrelated components of the

CONTACT Estela Pérez Luque  perezluque.estela1504@gmail.com  School of Engineering Science, University of Skövde, Skövde, Sweden.

© 2026 The Author(s). Published with license by Taylor & Francis Group, LLC

This is an Open Access article distributed under the terms of the Creative Commons Attribution License (<http://creativecommons.org/licenses/by/4.0/>), which permits unrestricted use, distribution, and reproduction in any medium, provided the original work is properly cited. The terms on which this article has been published allow the posting of the Accepted Manuscript in a repository by the author(s) or with their consent.

motion are typically considered: the end-effector path, the end-effector velocity, and the set of upper extremity joint angles configuration, which together define a reaching movement over time (Klein et al., 2022). The end-effector path describes the position of the index fingertip in space as it moves from the starting location to a target location, often represented as a sequence of points in space (Gong et al., 2018). Velocity is a measure of positional or angular change along a path over a period of time and can be measured in terms of a specific point on the body, e.g., the tip of a finger, or a joint, e.g., the elbow (Hamm, 2020). Arm joint configuration defines the specific angular relationship between the segments of the arm (shoulder, elbow, and wrist) that define the limb posture and coordination throughout the movement (Clark et al., 2020). Together, these components characterize the spatial and temporal aspects of a motion, forming what is commonly referred to as a trajectory, a continuous description of how the body, in this case an upper extremity, moves through space and time (Rudenko et al., 2020). Models that predict reaching motions should accurately predict at least one of these dimensions of the reaching trajectory and ideally should predict all three.

A range of modeling approaches has been developed to predict path, velocity, and posture (joint angles), both in isolation and together (Farahani et al., 2015; Kim et al., 2016; Wolf et al., 2020). These methods fall into the following groups: data-driven, optimization-based, and rule-based or heuristic approaches. Data-driven methods can involve using previously recorded motion data directly, either in its original form or rescaled. This approach serves as an alternative to more advanced prediction techniques that rely less directly on prior observations. Data-driven methods can also include statistical models, reinforcement learning, and artificial neural networks, which identify and/or learn patterns from recorded motion data, and then predict human motions that exhibit those patterns given limited initial conditions and task data (Porzio & Coraggio, 2025; Wang et al., 2019). Data-driven methods can excel when prediction contexts are similar to the training or observational datasets, but quickly diverge for novel prediction contexts (Cui et al., 2020; Xia et al., 2022). In contrast, optimization-based methods use a knowledge-based approach to identify a set of cost functions that represent features of human motion that are assumed to be controlled or prioritized in human motion. Cost functions may include muscle activity, energy consumption, comfort, dynamic effort, or joint displacements (Xiang et al., 2010; Yang et al., 2011; Zaman et al., 2021). Selected cost functions are integrated with optimization algorithms that aim to minimize or maximize the outputs of the cost functions for a given context, ideally resulting in an optimal motion prediction. Optimization-based methods typically perform better in novel prediction contexts than data-driven methods, as they are not as dependent on the specifics of previous observations. Lastly, heuristic methods also take a knowledge-driven approach, but instead of searching in a space of possible solutions based on cost functions, heuristic solvers apply a set of rules following specific patterns or regularities grounded in observations and theories of human motion to find a solution. Heuristic algorithms generally build on geometric operations involving points, distances, and angles in an iterative fashion, offering solutions that are more computationally efficient than data-driven or optimization-based approaches (Braun et al., 2021; Cao et al., 2023). Heuristic methods can include a behavioral dynamics approach to motion prediction, which predicts motion paths and velocity based on mathematical models derived from observations of human motion (Fajen & Warren, 2003). Thus, behavioral dynamics models are mathematical models based on observations and theories of human motion, like optimization-based approaches. Unlike optimization-based approaches, which search a space of possible trajectories to minimize a cost function, behavioral dynamics models generate a single prediction given a set of initial conditions and model parameters. Like optimization-based approaches, heuristic approaches have the potential to perform well in novel prediction contexts with the added potential of greater flexibility and computational efficiency.

For human motion prediction, the dominant prediction methods are data-driven and optimization-based methods. The choice between these methods typically relies on the type of data available and the specific context or goals of the prediction task. For these approaches, path, velocity, and joint angle predictions are typically integrated into a single prediction model, though some models predict velocity independent of path and joint angle predictions. Heuristic planners are relatively underexplored within fields investigating human motion, and there are currently no empirically validated heuristic-based approaches to human motion prediction that integrate path, velocity, and joint angle predictions. To

this end, we would like to explore heuristic planning methods to compare with the optimization-based method to determine their tradeoffs. Our proposed heuristic prediction approach integrates an empirically validated behavioral dynamics model for path prediction, a lowpass filter-based approach to velocity prediction, and a heuristic inverse kinematics solver that has been widely deployed in computer graphics but not validated for accuracy in human motion prediction. For the path, our model includes a modified version of the steering dynamics model (SDM) introduced by Fajen and Warren (Fajen & Warren, 2003, 2007), and later adapted by Lamb and colleagues to predict locomotion paths for a 2D reaching task (Lamb et al., 2017; Nalepka et al., 2019). While the 2D version of the SDM has demonstrated a good fit to a variety of human behaviors in 2D, we will implement a 3D variant to predict naturalistic reaching paths. For the velocity prediction component, the velocity model builds on early research into the relationship between muscle activation and reaching motions, where it was observed that physiological properties of muscles acted like a lowpass filter on observed velocity profiles (Gottlieb et al., 1989). Finally, we propose that the forward and backward inverse kinematics (FABRIK) solver can provide a solid basis for joint angle predictions given the velocity and path prediction of the lowpass velocity model and the SDM. The FABRIK solver has been widely deployed in computer graphics contexts, primarily for video game animations, but has also been deployed as a robot controller and demonstrates potential as an accurate method for accurate biomechanical predictions (Aristidou et al., 2016; Aristidou & Lasenby, 2011; Lamb et al., 2022; Moreno & Alcántara, 2022; Santos et al., 2021). Our combined heuristic model, named SFM (short for steering-FABRIK method), is a first-of-its-kind heuristic prediction model with the aim of providing an integrated prediction of path, velocity, and joint angle configuration over an entire reaching motion.

In this article, we will compare an initial formulation of the SFM to an established optimization-based modeling (OPM) approach. Understanding the differences between motion prediction models is essential for selecting the right approach in a given context. Different methods entail tradeoffs in accuracy, precision, generalizability, and computational cost. In this article, we will primarily focus on the relative potential of the SFM and OPM as regards accuracy. We will consider both how accurately the models predict specific individual motions and how well they reflect the patterns of variability in human motion. By comparing these models, researchers can make more informed choices tailored to their specific application, whether in robotics, ergonomics, rehabilitation, or animation.

The aim of the study is to compare two different motion prediction methods for modeling upper extremity reaching in 3D space. The OPM approach applied in this study uses cost functions related to all three components, i.e., end-effector path, end-effector velocity, and upper extremity joint configuration. The second is our proposed SFM heuristic approach. For the comparison, prediction output from OPM and SFM are validated against motion capture experimental data, evaluated across three motion components: path, velocity, and upper extremity joint configuration throughout the upper extremity reaching motion.

2. Methods

To compare the proposed SFM approach with an existing OPM approach, we collected a unique motion capture experimental dataset consisting of four unconstrained upper extremity reaching motions. Because this study is performed in the context of a project focused on methods for vehicle cabin design, we selected motions related to a vehicle cabin from the perspective of the driver.

2.1. Experimental collected data

A total of 10 (5 males and 5 females) participants (age: 27.5 ± 4 years) volunteered for the experiment. All of them were physically and mentally sound. They were right-handed and had no restrictions on their right arm during testing. All participants gave written informed consent for both participating in the study and publishing the data, and completed four tasks with three trials each.

A motion capture system with eight cameras (Motion Analysis Corporation, CA) was used to collect the right upper extremity motion data (60 Hz) (Figure 1(a)). Ten retroreflective markers were placed on



(a)



(b)



(c)

Figure 1. Lab experiments: (a) motion capture environment with an eight-camera system, (b) initial posture with both arms straight down, and (c) final posture of Task 2 (front view).

the subject's right half of the upper body, as shown in [Figure 1\(b,c\)](#). The markers were attached to the bony landmarks following the protocol (Cloutier et al., 2011).

All participants were instructed to “touch” four target points separately, assuming they were sitting in their driver's seat with the initial posture as the arms straight down ([Figure 1\(b\)](#)): the rearview mirror (Task 1), seat belt (Task 2), gear shifter (Task 3), and passenger seat (Task 4). Each participant was instructed to perform the abovementioned tasks one by one in the following order: (1) have a relaxed posture sitting on a chair, (2) reach the target point from the initial posture in (1), and (3) stop for 3 s at the target location and then return to the initial posture described in (1).

The Generator of Body Data (GEBOD) was used to create the subjects' anthropometric data (arm segment lengths) listed in [Table 1](#) based on the subject's gender, stature, and weight (Huaining et al., 1994). Markers were labeled, and their position curves were smoothed in Cortex (Motion Analysis Corporation, Rohnert Park, CA, USA). After the post-processing, the data were converted into a C3D file and became the input for Visual 3D (C-Motion Inc., Germantown, MD, USA). In Visual 3D,

Table 1. Anthropometric data of the right upper extremity.

Subject	Gender	Height (m)	Weight (kg)	Upper arm length (m)	Forearm length (m)	Hand length (m)
1	Male	1.87	110	0.318	0.266	0.207
2	Male	1.74	75	0.301	0.258	0.188
3	Male	1.89	90	0.324	0.278	0.201
4	Male	1.85	106	0.314	0.264	0.199
5	Male	1.88	77	0.326	0.282	0.199
6	Female	1.65	47	0.270	0.222	0.185
7	Female	1.48	46	0.230	0.200	0.170
8	Female	1.60	53	0.254	0.214	0.181
9	Female	1.58	48	0.252	0.212	0.179
10	Female	1.70	65	0.270	0.224	0.191

motion capture experimental data were utilized to build a model (upper arm, forearm, and hand), and all joint angles (the shoulder, elbow, and wrist joints) were calculated.

2.1.1. Skeletal model

The right upper extremity model is constructed with seven degrees of freedom (DOFs). Figure 2 shows Denavit–Hartenberg (DH) representations (Denavit & Hartenberg, 1955), and the corresponding DH parameters are shown in Table 2. The first three DOFs (q_1, q_2, q_3) represent the shoulder flexion, abduction, and rotation, respectively. The fourth DOF (q_4) corresponds to the elbow flexion. The final three DOFs (q_5, q_6, q_7) are the wrist flexion, deviation, and rotation, respectively. In the kinematic chain, l_1 corresponds to the upper arm length, l_2 to the forearm length, and l_3 to the hand length, which is reflected in Table 2 and Figure 2. The definitions of the DH parameters (θ, d, a, α) in Table 2 follow the original convention presented by Denavit and Hartenberg (1955).

2.2. Optimization-based prediction method

The right upper extremity motion is formulated as a nonlinear programming problem, shown in Equations (1)–(3) for the OPM, and the results of the optimization-based method are the end-effector path, velocity, and joint angle profiles and instantaneous upper extremity configuration. The optimization formulation was solved through the commercial software MATLAB. A local optimization solver, FMINCON, was selected to solve the nonlinear problem, and sequential quadratic programming was applied.

2.2.1. Optimization formulation

The control points (\mathbf{P}_c) of cubic B-spline curves for joint angles are design variables. The cost function is to minimize the joint displacements from the neutral position and maximize the end-effector velocity, shown as follows:

$$J = \int_0^T \sum_{i=1}^7 \frac{w_i (q_i(\mathbf{P}_c, t) - q_i^N)^2}{\left(\|\dot{\mathbf{P}}_{\text{end-effector}}(t)\|_2^2 + \alpha \right)} dt \quad (1)$$

where T is the total task time that is from the subject's experimental data, q_i^N is the i th neutral joint angles, $\dot{\mathbf{P}}_{\text{end-effector}}$ is a velocity vector of the end-effector, α is a positive constant that avoids the denominator to be zero, and 100 is used in this study. The neutral joint angles are defined by our previous research (Yang et al., 2004), representing a relatively comfortable posture. w_i is the i th objective function weight coefficient, where $w_1, w_2, w_5 \sim w_7$ are 0.4, and w_3 and w_4 are 0.6, respectively. Note that in the cost function, the reason to maximize the end-effector velocity is to prevent the zig-zag motion of the end-effector because the upper extremity model is a redundant system.

2.2.2. Constraints

The right upper extremity reaching motion is subject to time-dependent and time-independent constraints. For the time-dependent constraint, joint angle limits are applied to avoid hyperextension and hyperflexion. The i th joint angle limits are defined in Equation (2).

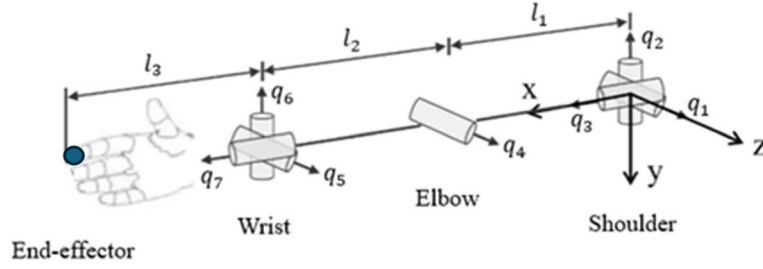


Figure 2. 3D right upper extremity model.

Table 2. DH table of the right upper extremity model.

Segment	DOF	θ (rad)	d (m)	a (m)	α (rad)
Shoulder	Shoulder _z (q_1)	0	0	0	$\pi/2$
	Shoulder _y (q_2)	$\pi/2$	0	0	$\pi/2$
	Shoulder _x (q_3)	$\pi/2$	Upper arm length (l_1)	0	$\pi/2$
Elbow	Elbow _z (q_4)	$\pi/2$	0	Forearm length (l_2)	0
Wrist	Wrist _z (q_5)	0	0	0	$\pi/2$
	Wrist _y (q_6)	$\pi/2$	0	0	$\pi/2$
	Wrist _x (q_7)	0	Hand length (l_3)	0	0

$$q_i^L \leq q_i(\mathbf{c}, t) \leq q_i^U \quad (2)$$

where q_i^L and q_i^U represent the i th lower and upper joint angle limits, respectively. The joint angle limits are listed in Table 3.

The time-independent constraints are the initial and final postures. The right upper extremity joint angles constrain the experimental data at the initial and final task, shown as

$$q_i(\mathbf{c}, t) = q_i^E(t), \quad t = 0, T \quad (3)$$

where q_i^E is the i th joint angle from experiments.

2.3. Heuristic prediction method (SFM)

The SFM heuristic method integrates three interconnected sub-models to simulate and predict human reaching motions in 3D space (Tables 4 and 5). First, the SDM predicts the heading of the end-effector as well as aligns the end-effector orientation with the goal hand pose orientation. Second, a velocity model predicts the distance the end effector travels along the predicted heading during each time step of the prediction. Finally, an arm joint angle configuration that places the end-effector in the newly predicted position and orientation while respecting joint constraints is predicted using the FABRIK inverse kinematics solver. The combined use of these three models enables the generation of full arm reaching motions in 3D space.

Table 5 outlines this integrated approach (SFM) in pseudocode.

2.3.1. Steering dynamics model (SDM)

The SDM, originally developed in cognitive science by Fajen and Warren (2003), is a behavioral dynamics model that predicts human steering behavior toward goals while navigating through space. The SDM predicts the change in heading of a system, e.g., the end effector of the arm, as it approaches a goal location. Thus, the SDM is a second-order differential equation based on a damped-mass spring model that describes changes in heading direction, ϕ , over time (Equation (4)). The angular acceleration, $\ddot{\phi}$, is influenced by the damping, b , stiffness controlling the strength of the goal attraction, k_g , the angular heading to the goal, ψ_g , from the current position, and a set of decay parameters, c_1 and c_2 , that modulated the effect of goal distance, d_g , on turning.

$$\ddot{\phi} = -b\dot{\phi} - k_g (\phi - \psi_g) (e^{-c_1 d_g} + c_2) \quad (4)$$

Table 3. Joint angle limits.

DOF	Lower limit (°)	Upper limit (°)
Shoulder _z (q_1)	-180	60
Shoulder _y (q_2)	-120	60
Shoulder _x (q_3)	-90	45
Elbow _z (q_4)	-130	10
Wrist _z (q_5)	-45	45
Wrist _y (q_6)	-45	45
Wrist _x (q_7)	-45	45

Table 4. Components of the SFM (heuristic method).

Motion component	SFM sub-models used	Function
Path	Steering dynamics model (Fajen & Warren, 2003)	Computes the spatial trajectory of the end-effector using the input velocity
Velocity	Adaptive lowpass velocity model (Gottlieb et al., 1989)	Defines the speed profile of the end-effector based on its distance to the target
Upper extremity configuration	FABRIK (Aristidou & Lasenby, 2011)	Determines the joint angles needed to achieve the desired end-effector path

Table 5. Input parameters (left) and pseudocode for the SFM algorithm (right), outlining the iterative prediction of hand path, velocity, and arm joint configuration at each timestep.

<p>Input: Initial joint angles, Initial end-effector position, goal position, Initial velocity, estimated peak velocity.</p> <p>Constraints: Joint angle limits. Tuned SFM parameters (see Table 6)</p> <p>Parameters: g_{pos} = goal position. h_{pos} = end-effector position. h_{ort} = end-effector bone orientation. h_{fwd} = forward vector of end-effector heading. h_{vel} = end-effector velocity. h_{dist} = distance (meters) between h_{pos} and g_{pos}. h_{err} = angular error between h_{fwd} and vector from h_{pos} to g_{pos}. $\{q_1, q_2, \dots, q_7\}$ = set of joint angles defining the arm configuration. $m = \{g_{pos}, h_{pos}, h_{ort}, h_{fwd}, h_{vel}, h_{dist}, h_{err}, \dots, \{q_1, q_2, \dots, q_7\}\}$ $M = \{m_1, m_2, \dots, m_n\}$ where n is the length of the final predicted motion trajectory.</p>	<p>Pseudocode: $n = 1$ Initialize M with current state of arm, m_n. While ($h_{dist} > 0.01$) $n = n + 1$ Estimate change in h_{fwd} (SDM). Estimate change in h_{ort} (SDM). Estimate change in h_{vel} (low-pass filter velocity model). Predict next h_{pos} and h_{ort} based on estimated changes in h_{fwd}, h_{ort}, and h_{vel}. Estimate new $\{q_1, q_2, \dots, q_7\}$ given current $\{q_1, q_2, \dots, q_7\}$ and predicted h_{pos} and h_{ort} (FABRIK). Calculate new h_{dist} and h_{err}. Set m_n to updated state estimates. Add m_n to list of M. End</p>
---	---

A detailed description of the original model, its derivation, and validation can be found in Fajen and Warren (2003). The parameters used were selected through manual testing across a range of values to ensure plausible steering trajectories for the reaching tasks.

While the SDM was originally formulated in 2D, for the current comparison, we extended the model to 3D space using quaternion algebra, enabling smooth orientation transitions in 3D space. The original SDM formulation assumes a single plane of rotation and where the predicted headings are defined relative to the plane normal centered on the predicted system's position. The generalized 3D SDM makes the angle-axis representation of the system's heading explicit so that the axis of rotation can change throughout the path. To select a single axis of rotation at each timestep, the 3D SDM uses a quaternion representation of the hand's current motion heading to define ϕ relative to an axis of rotation, v_{hr} . The axis of rotation v_{hr} , was defined by treating the hand's forward motion as the vector, v_{hf} , defined by the normalized difference between the hand's current position and its previous position. An arbitrary

orthogonal vector, v_{ho} , was defined as $v_{ho} = v_{hf} \times v_{wu}$ where $v_{wu} = \begin{bmatrix} 0 \\ 1 \\ 0 \end{bmatrix}$ representing a global vertical vector, thus $v_{hr} = v_{hf} \times v_{ho}$. Thus, the orthonormal basis of the current motion heading can be defined as $[v_{hf}, v_{ho}, v_{hr}]$ from which the quaternion q_h can be derived. A similar approach to the goal heading

starts with the vector, v_{gf} , defined by the normalized difference between the hand's position and the goal position. The orthogonal vector is defined as $v_{go} = v_{gf} \times v_{wu}$ and the rotational vector $v_{gr} = v_{gf} \times v_{go}$, from which a quaternion to the goal, q_g , can be derived. The rotation from q_h to q_g is then defined as $q_{hg} = q_g q_h^{-1}$ and enforce the shortest rotation path (Equation (5)):

$$q_{hg} \begin{cases} -q_{hg}, & \text{if } (q_g \cdot q_h) < 0 \\ q_{hg}, & \text{otherwise} \end{cases} \quad (5)$$

Standard quaternion algebra allows for the derivation of the desired angular rotation, $(\phi - \psi_g)$, from q_{hg} , as well as the relevant axis of rotation, v_{hgr} , used to rotate from one heading to the other.

At each timestep of the prediction, a plane of rotation, defined by the plain normal vector, v_n , and the end-effector location, h_{pos} , was identified, and the goal heading was calculated relative to that plane. Continuous updating of the plane of rotation allows the 3D SDM to accommodate changes in task and environment, including obstacles. The model output is a predicted change in heading that can be used to derive a positional change once the velocity is predicted.

2.3.2. Adaptive lowpass velocity model

One approach to velocity prediction is to assume a total time to arrive at the reach target, typically based on distance and difficulty of the reach task, combined with some form of Fitts Law (Fitts, 1954). However, timing estimates can be highly variable and can be affected by active movement, suggesting that while time estimates may play a role in human motion generation, they may be too noisy to play the strong role assumed in these types of velocity prediction models. We propose a novel approach to velocity prediction that does not assume accurate time estimates and instead builds on observed neuromuscular properties combined with an estimate of braking ability grounded in Ecological Psychology (Gibson, 1979; Gottlieb et al., 1989; Harrison et al., 2016). Our proposed model leverages the observation that muscle activations during reaching can be modeled as a lowpass filter applied to an increasing or decreasing activation of motoneuron pools (Gottlieb et al., 1989). Thus, the velocity prediction model is a simple damped-mass spring model that stands in for the detailed muscle dynamics of the arm system (Equation (6)):

$$\ddot{v} = -b_v \dot{v} - k_v (v - (v_{peak} \times s)) \quad (6)$$

where v is velocity, b_v is a frictional damping force, and k_v is a stiffness term. The peak velocity is estimated prior to prediction using a linear regression model based on the distance to the goal, which was the most predictive variable among a wide set of motion and anthropometric parameters. This variable showed a strong correlation with peak velocity ($R=0.70$), and its use enables prediction without requiring subject-specific measurement. The resulting regression model is (Equation (7))

$$v_{peak} = 1.1241 \times d_g + 25.788 \quad (7)$$

The current level of activation $\{s \in \mathbb{R} \mid 0 \leq s \leq 1\}$ modulates the maximum value of \ddot{v} and depends on the system's distance to the target and current ability to stop, where the ability to stop is estimated based on the current velocity and the settling time of the system described by

$$\tau = \frac{\log(t_{resp})}{\sqrt{k_v}} \quad (8a)$$

$$acc_{est} = v / \text{round}(\tau \times f) \quad (8b)$$

$$b_d = (v \times \tau) + \left(\frac{acc_{est}}{2} + \tau^2 \right) \quad (8c)$$

assuming that the velocity equation settles to a $\ddot{v} = 0$, with a transient response of 5% (t_{resp}), and that the system is critically damped. In Equation (8b), f is a framerate value (1/frames per second) indicating granular precision where higher frames per second increase braking distance estimate precision. For this study, we decided on 200 frames per second or $f = 0.005$, a value at which estimates did not meaningfully change. The resulting settling time estimate is used to determine the rough minimum

stopping distance, b_d , given the current state of the system and the equation of motion defined by Equation (8c), specifically an estimate of displacement. The ratio, described in Equation (9):

$$b_a = \frac{b_d}{d_g} \quad (9)$$

thus characterizes the ability of the agent to stop, b_a , before reaching the target if the activation signal is set to 0, where $b_a < 1$ indicates that the system will overshoot the target resulting in a collision and $b_a \geq 1$ indicates that the system is able to stop at or before reaching the target. Thus, given the current activation level, s_{cur} , a new value, s , can be estimated using an adaptive low-pass filter formulation (Equation (10)):

$$s = \begin{cases} s_{cur} - \frac{s_{cur}}{d_g/c_3}, & \text{if } b_a < 2 \\ s_{cur} + \frac{s_{cur}}{d_g/c_3}, & \text{otherwise} \end{cases} \quad (10)$$

where c_3 is a constant value modulating the effect of distance on the filtered s value. The value of $b_a < 2$ was selected because the low-pass filter formulation does not allow for an instantaneous reduction of s to 0. In this way, the velocity model predicts the change in velocity of the hand given only the state of the reaching system and an expected maximum velocity. The neuromuscular properties of the system are represented by a simple damped-mass spring system and a low-pass filter combined with a mathematical description of the system's stopping ability to stop, i.e., its stopping affordance. When combined with the predicted changes in heading and velocity are taken together, one can predict the change in hand position from the current point in the reaching trajectory. The predicted hand position can then be passed to the FABRIK solver to predict the remaining arm joint configuration.

2.3.3. FABRIK solver

To determine the right arm joint angle configuration that follows the predicted end-effector path generated by the SDM and velocity models, the FABRIK model is employed. FABRIK is a heuristic iterative algorithm that solves the inverse kinematics problem by adjusting joint positions based on simple geometric rules (Aristidou & Lasenby, 2011). Each joint is updated by projecting it onto a line defined by its neighbor and preserving segment lengths, making it computationally efficient and free from the singularities that affect Jacobian-based methods.

The algorithm operates in two stages per iteration: a forward reaching phase where the end-effector is placed at the target position and joint positions are recalculated backward along the chain, followed by a backward reaching phase where the base joint is reset to its original position and joint positions are updated outward toward the end-effector (Figure 3). This cycle continues until the end-effector reaches the target within a predefined tolerance. FABRIK also supports joint constraints, and in this implementation, the same joint angle limits as those used in the OPM were applied to ensure a fair comparison (Table 3).

In order to ensure biomechanically realistic solutions, it is critical that the FABRIK algorithm can accommodate joint angle constraints consistent with human joint types. Joint angle constraints are typically introduced locally to each joint as needed in both the forward and backward phases of the algorithm (Aristidou et al., 2016; Aristidou & Lasenby, 2011; Moreno & Alcántara, 2022; Santos et al., 2021). The approach for constraining each joint varies depending on the joint type. For 2D and 3D joint constraints, as in the wrist and simplified shoulder model, the general approach involves determining whether the solution is inside or outside of a joint angle defined solution volume, sometimes called a "reach cone" (Aristidou et al., 2016; Wilhelms & Gelder, 2001). If not, then the local solution is projected to the nearest feasible solution within the solution cone. For a 1D constraint, as in the elbow, the approach is similar but requires additional consideration to avoid getting trapped in local minima (Aristidou et al., 2016; Moreno & Alcántara, 2022). The simulations below used relevant approaches detailed in (Aristidou et al., 2016; Moreno & Alcántara, 2022; Wilhelms & Gelder, 2001).

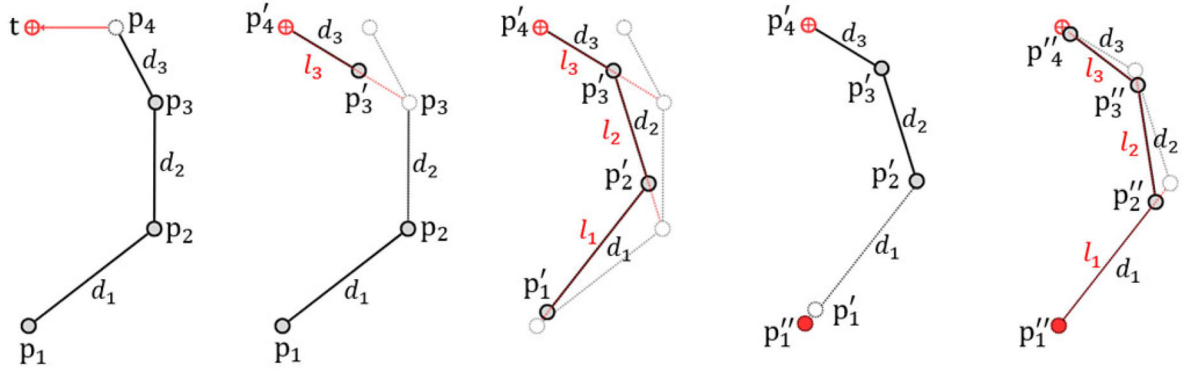


Figure 3. Illustration of a full iteration cycle of the FABRIK algorithm for a 4-joint chain.

2.3.4. Parameter definition and selection

The SFM heuristic method includes a limited number of model parameters associated with the SDM, the velocity model, and FABRIK. These parameter values were selected through iterative testing on the full dataset by examining their qualitative and quantitative effects on predicted trajectories and velocity profiles, with the aim of ensuring both numerical stability and biomechanically plausible upper-limb reaching behavior. Parameter ranges were explored to avoid oscillatory path behavior in the SDM, unrealistically abrupt accelerations or prolonged deceleration tails in the velocity model, and non-convergent or constraint-violating solutions in the inverse kinematics stage.

For the SDM, the values were based on previous literature using the model in a locomotion context (Fajen & Warren, 2003, 2007). In previous studies the damping value b , was treated as free parameter, however, to ensure that the heading equation is critically damped we use the critical damping formula defined in Table 6. The values for k_g and c_1 are taken from previous papers (Fajen & Warren, 2003, 2007) and c_2 was reduced to eliminate a tendency of the simulation model to turn too early. This later change affects the parameter that ensures that the model's turning rate does not go to zero at large distances, and the difference in values between our simulations and previous literature likely relates to differences in reaching and walking modes of motion.

For the velocity model, parameters governing acceleration and deceleration phases were adjusted to ensure a peaked velocity profile consistent with experimental observations. The final parameter set ensured that the predicted peak velocity matched the regression-based estimate while maintaining a smooth deceleration phase as the target was approached, a characteristic commonly reported in human motor control studies. In this proof-of-concept phase for the velocity model, parameterization values are not directly derived from biomechanical properties of participants. Future research will investigate how best to explicitly parameterize the velocity model based on the muscle and neuron pool dynamics of individual actors (Corcos et al., 1989; Gottlieb et al., 1989).

For the inverse kinematics stage, convergence tolerances and iteration limits were selected to ensure stable solutions within each simulation time step while respecting joint angle constraints. Looser tolerances reduced computational cost but introduced noticeable end-effector inaccuracies, whereas overly strict tolerances increased computation time without measurable gains in prediction accuracy. The selected values balance computational efficiency with the biomechanical feasibility of the predicted arm configurations.

The parameter values used across all simulations are summarized in Table 6.

2.4. Data analysis

2.4.1. Accuracy evaluation

The accuracy of the two prediction methods, OPM and SFM, was evaluated against experimental motion capture data. The analysis focused on three motion components: end-effector (hand) path, end-effector velocity profile, and arm joint configuration over time. For each of these, the corresponding

Table 6. Parameters used in the SFM.

SDM parameters:	Stiffness toward goal attraction: $k_g = 7.5$ Damping coefficient: $b = 2 \times \sqrt{k_g}$ Goal distance-dependent decay: $c_1 = 0.40$ Goal turning-dependent decay: $c_2 = 0.01$
Velocity parameters:	Frictional damping coefficient: $b_v = 2.0$ Peak velocity convergence stiffness: $k_v = 350$ Acceleration distance-dependent decay: $c_3 = 2.75$
FABRIK parameters:	End-effector convergence tolerance: 0.01 Maximum number of iterations per time step: 50

Note: All parameters were kept constant across subjects and tasks.

time series data were preprocessed, normalized, and quantitatively assessed using two metrics: root mean square error (RMSE) and dynamic time warping (DTW).

RMSE is a widely used metric for evaluating the accuracy of prediction models. It quantifies the average magnitude of the error between predicted and observed values at each time point. However, RMSE treats motion profiles as purely numerical sequences and does not account for differences in the geometric shape of the movement. This can lead to misleading conclusions when comparing complex trajectories or when trajectories differ in spatial or temporal scale and alignment. To address these limitations, we applied the DTW method as a complementary evaluation metric. Unlike RMSE, DTW compares sequences by non-linearly aligning them in time, allowing for shifts, delays, or differences in duration (Senin, 2008). This makes DTW particularly suitable for analyzing 3D human motion, where similarities in trajectory shape can be obscured by differences in spatial or temporal scale and alignment (Cleasby et al., 2019). To illustrate the differences, Figure 4 shows a conceptual example contrasting RMSE (Euclidean distance) and DTW alignment.

In this context, it is important to note that low RMSE values do not necessarily correspond to low DTW values, and vice versa. RMSE measures point-by-point differences between predicted and observed trajectories and can therefore remain low even when the overall shape or timing of the movement differs, as long as the points of each trajectory, on average, are near one another. DTW, on the other hand, evaluates the similarity of entire trajectories and is more sensitive to differences in how the movement evolves over time, such as shifts in timing or changes in trajectory shape. As a result, DTW tends to penalize trajectories that require substantial temporal realignment to achieve a good match. This includes movements with delay, prolonged deceleration phases, or differences in the timing of peak velocity, even when the overall spatial error is small.

For the current comparison study, DTW provides a cost matrix representing the distance between each point in a predicted sequence and each point in the observed trajectory. The cost matrix then represents all possible alignments between the two sequences. Given this matrix, one can compute an optimal warping path, consisting of the best alignment between the two datasets, by finding the path through the cost matrix that has the lowest summed distance value. The resulting, i.e., the minimal summed distance, DTW value represents the minimal cumulative cost required to align the sequences (Senin, 2008). A baseline DTW value was derived by applying DTW task-wise to observed data. Thus, each trajectory in a task was individually compared to every other trajectory produced for that task. The average and range of these DTW values for each task provide an expected similarity range for the prediction data. We reason that DTW values within this range can be considered as similar to a specific observed data as any other human trajectory for that task would be. This is a minimal success criterion providing the upper bounds for what might be considered a successful prediction. In the ideal case, the DTW value for a successful prediction of any specific observed trajectory would approach 0.

To ensure that DTW reflects shape similarity rather than magnitude differences, each sequence was centered by subtracting its mean and scaling it by normalization using the Euclidean (L2) norm (Latash, 2010). This normalization step removes global offset and amplitude variation, aligning sequences to emphasize their temporal and geometric structure.

2.4.2. Evaluation of modeled inter-subject variability

In addition to evaluating the accuracy of each method against experimental data, a complementary analysis was performed to assess the extent to which each method preserved natural inter-individual

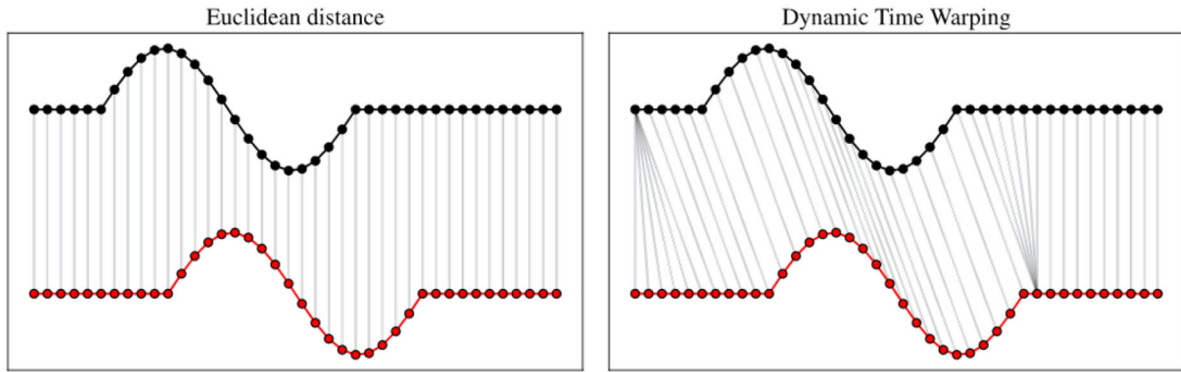


Figure 4. Visual comparison between RMSE (left) and DTW (right) for evaluating time series similarity. RMSE compares values at the same time steps, while DTW allows for flexible temporal alignment. Adapted from Tavenard (2021).

variability in movement. The goal of this analysis was to determine whether the predictions generated by each method could reflect the behavioral differences observed across different subjects.

This was achieved by comparing motion sequences between all subjects within each dataset (experimental, OPM, and SFM). Pairwise RMSE and DTW values were calculated for every subject-to-subject combination within each group (e.g., real-to-real, OPM-to-OPM, and SFM-to-SFM). These within-group comparisons provided a quantitative measure of the inter-subject variability generated by each method.

Rather than comparing predictions to experimental data, this analysis focused on evaluating the variation across subjects within each dataset. The resulting distributions of variability scores establish a baseline for interpreting each method’s ability to simulate human motion diversity.

2.4.3. Preprocessing and normalization

Before calculating RMSE and DTW, all motion sequences underwent the same preprocessing. First, the 3D position of the end-effector (right hand tip) was computed for each frame for both observed and simulated data. From these positions, absolute velocity curves were derived. In the SFM predictions, the velocity occasionally became asymptotic near the target. To prevent this low-motion “tail” from skewing temporal alignment, the sequences were truncated when velocity dropped below 5% of the peak value (Sethi et al., 2017). Because the proposed SFM method does not rely on an initial estimate of movement duration, its predicted trajectory times often differed from those of the OPM and the observed data. To enable comparison, all data were resampled onto a percentage-normalized time axis, ranging from 0% to 100% of task duration. This allowed consistent application of both RMSE and DTW across subjects and methods, regardless of execution speed or original recording length. Two trials were removed as outliers because their peak velocity was more than 2 standard deviations above the average velocity for their respective tasks.

At this point, RMSE was computed at three levels: per frame, per subject, and per task. As described above, prior to DTW calculation, each sequence was normalized by subtracting its mean value and scaling to unit L2 norm. This allowed DTW to focus on the shape of the motion profiles rather than absolute differences in magnitude or offset.

Each motion component (path, velocity, and arm configuration) was processed and analyzed using the same processing and analysis pipeline, scaled for the component’s dimensionality. The path was represented as a 3D multivariate time series (x, y, z), capturing the Cartesian trajectory of the end-effector. Velocity consisted of a univariate time series representing the speed magnitude of end-effector movement over time. Arm configuration was modeled as a 7D multivariate time series composed of seven joint angles, one for each degree of freedom in the right upper extremity model (see Figure 2). Table 7 summarizes the data structure for each motion component, clarifying their dimensionality and how they are represented for the analysis.

RMSE was computed for each motion component by comparing their time series on a per-dimension basis (e.g., velocity, each path axis, or each joint angle). In contrast, DTW was applied to each

Table 7. Data structure of the analyzed motion components.

Motion component	Data type	Description
Path	3D multivariate time series	Cartesian position (x, y, z) of the end-effector
Velocity	1D univariate time series	Magnitude of end-effector velocity over time
Arm joint configuration	7D multivariate time series	Joint angles for the 7-DOF right upper extremity model

multivariate time series as a whole, providing a similarity score characterizing the similarity of the respective n -dimensional shapes.

3. Results

Results are reported individually for each motion component.

3.1. End-effector path

Figure 5(a–c) displays the end-effector paths of all ten subjects in Task 4, comparing observed paths to predictions from the OPM and SFM methods. Each colored line represents a different subject, and the same color-subject pair is used across all visualization methods. In this task, observed paths exhibit a range of spatial patterns, reflecting diverse individual strategies. OPM predictions generally follow a more arc-like path, deviating in some cases from the observed path direction and curvatures. SFM predictions appear slightly more adapted to individual variations in path direction and curvature for several subjects.

Table 8 presents the quantitative evaluation of spatial path prediction accuracy using RMSE and DTW metrics across all four tasks. RMSE measures the overall spatial error between the predicted and observed end-effector paths, while DTW reflects differences in the shape of the paths. The comparison of RMSE values shows that SFM outperforms OPM with lower RMSE values in Tasks 1 (23.4 for SFM vs. 31.3 for OPM) and 4 (21.1 for SFM vs. 25 for OPM) and shows nearly equal performance in Task 3. Only in Task 2, OPM achieves a slightly better RMSE. DTW values reveal a similar trend. SFM matches or exceeds OPM with closer to observed shape similarity in Tasks 1 and 4. Both methods perform equally in Task 3, and OPM slightly outperforms in Task 2.

3.1.1. Best and worst path predictions

Figure 6 shows the best and worst path planning predictions for each method based on the DTW metric. The top row presents the best-matching predictions. In both cases, the predicted trajectories closely follow the observed paths. The bottom row shows the least accurate predictions for each method, where predictions show visible differences in the trajectory's initial direction, spatial curvature, and endpoint location, as can be seen for the SFM prediction.

3.1.2. Modeled inter-subject path variability

Table 9 reports the modeled path planning inter-subject variability for the observed and predicted data using RMSE and DTW metrics. The observed motions exhibit the highest variability across all tasks in magnitude and shape. Among the two methods, SFM consistently shows higher mean and standard deviation values than OPM across both metrics, meaning its variability is greater and ultimately more similar to the observed variability in magnitude and path shape. This indicates that SFM better captures the natural differences in path planning across individuals.

3.2. End-effector velocity

Figure 7(a–c) shows the absolute velocity curves for all ten subjects performing Task 1. The recorded curves typically display a rapid acceleration phase followed by a smooth deceleration as the hand reaches the target position. Individual deceleration phases regularly exhibited one or more short periods of acceleration prior to reaching the target (see Figure 7(a)). Occasionally, a similar moment of deceleration occurred during the initial acceleration phase. OPM predictions produce smooth and symmetric

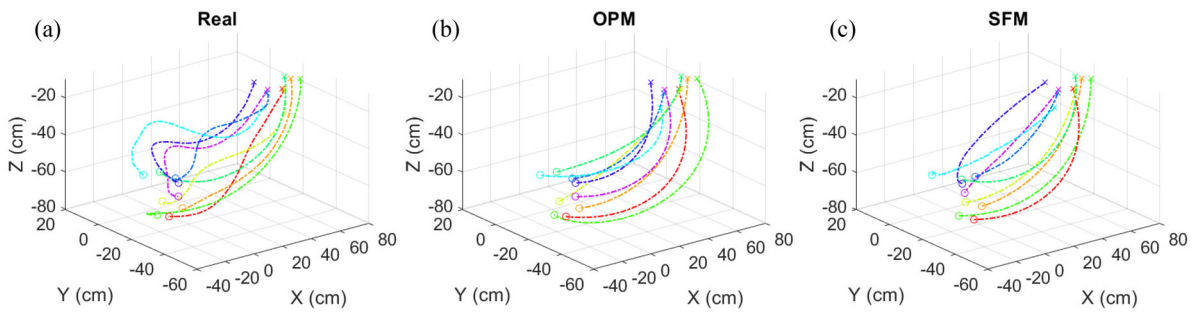


Figure 5. End-effector path of all subjects for Task 4: (a) experimental data, (b) OPM predictions, and (c) SFM predictions. Each trajectory corresponds to a different subject and the subject identity is consistent across all plots. Circles denote starting positions; crosses indicate end points.

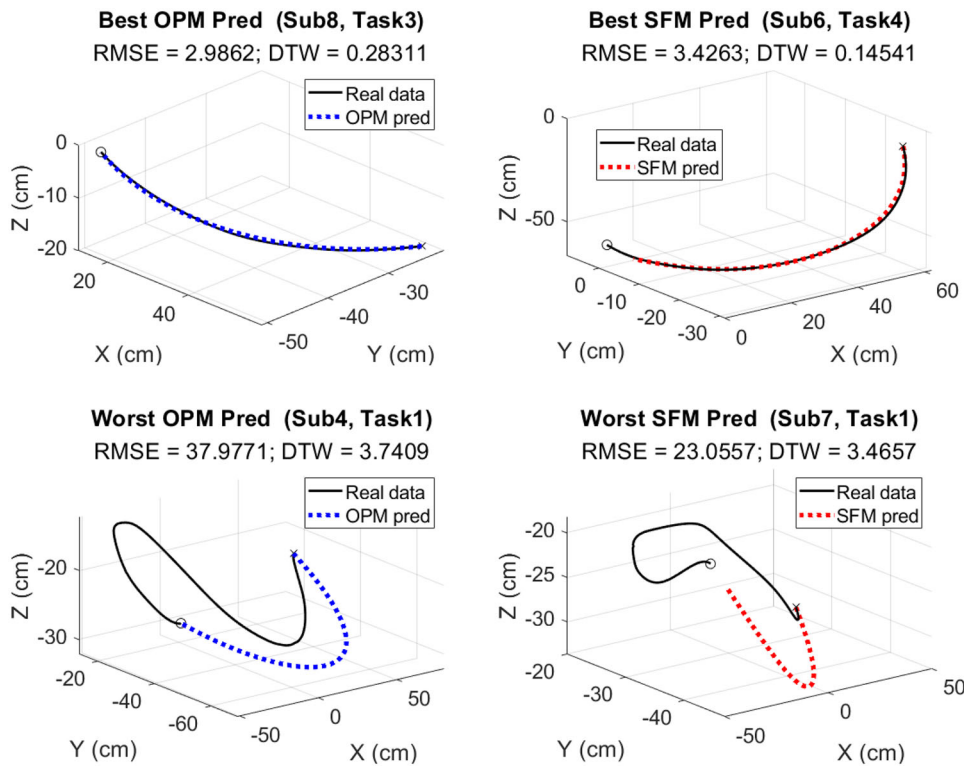


Figure 6. Examples of best (top) and worst (bottom) path predictions for the OPM (left) and SFM (right) methods, based on the DTW evaluation metric. Note: Axes are scaled individually for each subplot to enhance visualization of the trajectory shape. The examples correspond to different subjects and tasks and are intended for qualitative illustration only; quantitative comparisons are based on RMSE and DTW values reported in the text.

Table 8. Summary of path prediction results: RMSE and DTW values across all tasks.

		Task 1		Task 2		Task 3		Task 4	
		OPM	SDM	OPM	SDM	OPM	SDM	OPM	SDM
RMSE	Mean (SD)	31.3 (8.9)	23.4 (5.3)	19.1 (7.2)	22.3 (8.3)	14.3 (6.1)	14.5 (5)	25 (6)	21.1 (8.2)
	Std error	2.8	1.7	2.4	2.8	1.9	1.6	2.0	2.7
	Best pred	Sub 8	Sub 8	Sub 7	Sub 9	Sub 8	Sub 1	Sub 1	Sub 5
	Worse pred	Sub 5	Sub 4	Sub 3	Sub 4	Sub 10	Sub 6	Sub 2	Sub 6
DTW	Mean (SD)	2.4 (0.9)	2 (0.8)	1 (0.4)	1.2 (0.4)	1.3 (0.6)	1.3 (0.4)	1.8 (0.5)	1.5 (0.8)
	Std error	0.3	0.3	0.1	0.1	0.2	0.1	0.2	0.3
	Best pred	Sub 6	Sub 6	Sub 7	Sub 1	Sub 8	Sub 1	Sub 5	Sub 5
	Worse pred	Sub 4	Sub 7	Sub 3	Sub 4	Sub 10	Sub 6	Sub 8	Sub 9

RMSE is shown in cm. Bold values indicate better performance.

Table 9. Modeled inter-subject variability for path predictions.

	Task 1		Task 2		Task 3		Task 4	
	RMSE	DTW	RMSE	DTW	RMSE	DTW	RMSE	DTW
Real	31.8 ± 9.9 (11.5–53.9)	2.3 ± 0.6 (0.5–3.7)	25.9 ± 7.2 (16.1–45.6)	1.2 ± 0.5 (0.4–2.4)	28.1 ± 8.5 (11.8–44.8)	2.0 ± 0.6 (0.6–3.1)	28.2 ± 9.2 (13.3–54.8)	2.0 ± 0.7 (0.4–3.0)
OPM	22.0 ± 8.4 (5.4–39.0)	1.5 ± 0.7 (0.2–2.6)	23.8 ± 8.7 (8.2–48.9)	0.9 ± 0.5 (0.2–1.9)	20.9 ± 7.3 (8.1–34.9)	1.1 ± 0.8 (0.1–2.5)	24.7 ± 9.7 (7.9–48.5)	1.1 ± 0.5 (0.1–2.0)
SFM	25.9 ± 8.9 (8.7–46.4)	1.6 ± 0.6 (0.3–2.5)	25.9 ± 8.2 (7.0–39.2)	0.9 ± 0.4 (0.2–1.7)	21.3 ± 7.9 (5.7–36.6)	1.3 ± 0.6 (0.2–2.5)	19.6 ± 6.1 (7.1–32.0)	1.2 ± 0.7 (0.1–2.2)

RMSE and DTW are reported as mean ± SD (min–max). RMSE is shown in cm. Bold indicates the method with an average closer to observed values.

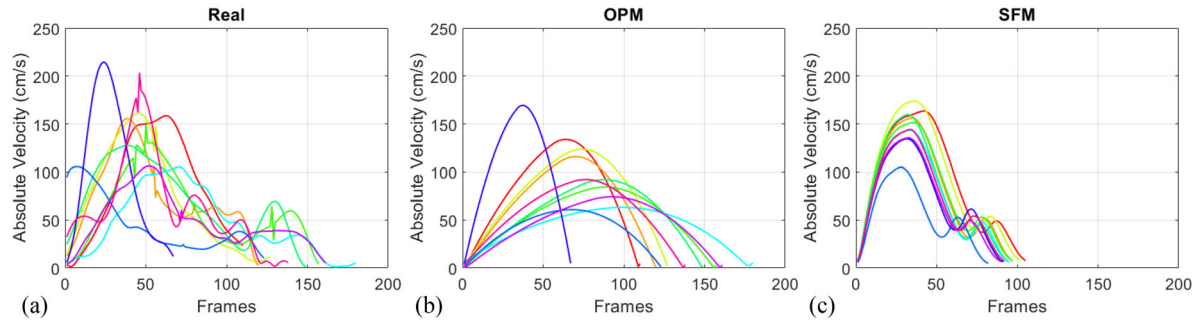


Figure 7. End-effector velocity profiles of all subjects for Task 1: (a) experimental data, (b) OPM predictions, and (c) SFM predictions. Each curve corresponds to a different subject, and the same subject correspondence is consistent across all plots.

Table 10. Summary of velocity prediction results: RMSE and DTW values across all tasks.

		Task 1		Task 2		Task 3		Task 4	
		OPM	SFM	OPM	SFM	OPM	SFM	OPM	SFM
RMSE	Mean (SD)	39.9 (11.4)	34 (9.3)	30.9 (14.9)	47.1 (15.9)	24.7 (8.4)	26.5 (9.3)	31.2 (15.9)	29 (10.1)
	Std error	3.6	3.0	5.0	5.3	2.7	3.0	5.3	3.4
	Best pred	Sub 1	Sub 2	Sub 2	Sub 5	Sub 4	Sub 7	Sub 7	Sub 5
	Worse pred	Sub 8	Sub 1	Sub 9	Sub 3	Sub 3	Sub 6	Sub 2	Sub 1
DTW	Mean (SD)	2.6 (2.1)	1.6 (1.2)	1.1 (0.5)	1.2 (0.4)	2.3 (1.2)	2.3 (0.8)	1.9 (0.8)	1.4 (0.5)
	Std error	0.7	0.4	0.2	0.1	0.4	0.3	0.3	0.2
	Best pred	Sub 1	Sub 1	Sub 3	Sub 2	Sub 2	Sub 1	Sub 5	Sub 4
	Worse pred	Sub 7	Sub 7	Sub 9	Sub 7	Sub 9	Sub 8	Sub 2	Sub 6

RMSE is shown in cm/s. Bold values indicate better performance.

bell-shaped curves, generally underestimating the peak velocities (see Figure 7(b)). On the other hand, SFM predictions typically exhibit a closer visual match to the shape and magnitude of the observed data's velocity curves, especially during deceleration, though SFM tended to reach the target earlier than was observed in the recorded data (see Figure 7(c)).

Table 10 summarizes the velocity prediction accuracy across all four tasks using two evaluation metrics: RMSE, measuring the overall amplitude errors, and DTW, measuring the profile shape similarity. A task-by-task comparison reveals that, according to the RMSE evaluation metric, SFM outperforms OPM in Task 1 (with an RMSE value of 34 compared to 39.9) and Task 4 (29 vs. 31.2). On the other hand, OPM achieves lower RMSE in Task 2 (30.9 vs. 47.1) and Task 3 (24.7 vs. 26.5), indicating a better match of overall (average) velocity magnitude and task duration.

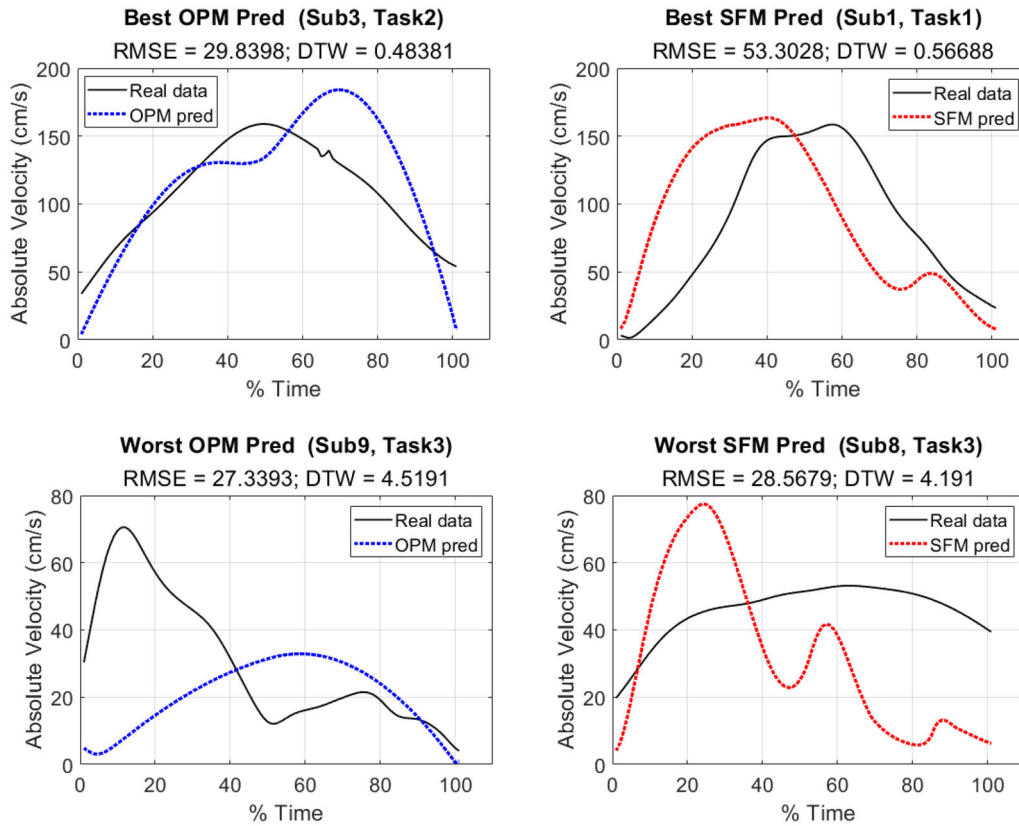
When looking at DTW values, SFM generally shows better or equivalent performance compared to OPM. Specifically, in Task 1 and Task 4, SFM clearly outperforms OPM with lower DTW values (1.6 vs. 2.6 and 1.4 vs. 1.9, respectively). Task 3 shows identical DTW values for both methods (2.3), and in Task 2, OPM has a slightly lower DTW (1.1 vs. 1.2), indicating a very close match in curve shape between the two methods for that task.

Table 11 presents the average peak velocities across subjects for each task. The observed data exhibit different peak velocities depending on the task, with Task 2 showing the highest peak on average (152.8 cm/s). Compared to the observed data, OPM underestimates the peak velocity in all tasks, with

Table 11. Average peak velocity values per method across all tasks in cm/s.

	Task 1	Task 2	Task 3	Task 4
Average peak vel observed (SD)	148.7 (38.9)	152.8 (30.4)	82.9 (24.4)	111.1 (29.5)
Average peak vel OPM (SD)	101.0 (34.4)	132.1 (34.6)	57.2 (24.4)	78.6 (23.5)
Average peak vel SFM (SD)	146.7 (19.2)	140.6 (14.1)	79.7 (13.3)	117.3 (13.6)

Bold indicates the method with an average peak velocity closer to observed values.

**Figure 8.** Examples of best (top) and worst (bottom) velocity predictions for the OPM (left) and SFM (right) methods, based on the DTW evaluation metric.**Table 12.** Modeled inter-subject variability in velocity profiles for each task.

	Task 1		Task 2		Task 3		Task 4	
	RMSE	DTW	RMSE	DTW	RMSE	DTW	RMSE	DTW
Real	43.5 ± 18.2 (16.5–95.1)	2.4 ± 2.0 (0.4–9.1)	46.4 ± 15.4 (12.9–76.9)	1.0 ± 0.5 (0.3–2.5)	32.4 ± 10.2 (10.9–57.7)	2.7 ± 1.5 (0.6–7.0)	36.2 ± 14.0 (15.2–74.9)	2.0 ± 0.8 (0.4–4.3)
OPM	27.8 ± 18.8 (2.5–73.9)	0.2 ± 0.1 (0.2–0.4)	30.8 ± 17.5 (4.0–69.1)	0.3 ± 0.1 (0.1–0.5)	16.2 ± 9.0 (0.7–37.2)	0.4 ± 0.2 (0.0–1.1)	19.8 ± 11.0 (3.5–45.0)	0.3 ± 0.1 (0.2–0.7)
SFM	16.0 ± 10.4 (2.8–45.8)	0.5 ± 0.3 (0.1–1.1)	21.0 ± 9.9 (4.9–45.6)	0.8 ± 0.3 (0.3–1.6)	17.9 ± 8.2 (3.1–41.6)	1.4 ± 0.7 (0.3–3.2)	15.4 ± 7.3 (1.9–29.9)	0.8 ± 0.4 (0.2–1.6)

RMSE and DTW are reported as mean ± SD (min–max). RMSE is shown in cm/s. Bold indicates the method with an average closer to observed values.

an average deviation of 31.6 cm/s, and reaching a maximum underestimation of 47.7 cm/s in Task 1. In contrast, SFM matches the experimental data more closely, with an average deviation of 2.8 cm/s.

3.2.1. Best and worst velocity predictions

To further illustrate the velocity prediction performance, Figure 8 shows each method's best and worst velocity predictions, comparing the observed and predicted profiles for the corresponding subjects and tasks. The top row displays the best cases based on the DTW metric, where both OPM and SFM predicted curves follow the general shape well. The bottom row shows the worst cases, where both methods' predictions deviate from the curve shape of the observed data.

3.2.2. Modeled inter-subject velocity variability

Table 12 shows how observed velocity profiles exhibit substantially higher variability in both magnitude (RMSE) and shape (DTW) across all tasks. In contrast, both OPM and SFM consistently produce lower variability, suggesting more uniform predictions across subjects. OPM generally reproduces a higher level of variability than SFM, especially in terms of RMSE values, suggesting that its predictions better reflect the magnitude differences in how individual participants perform the tasks. SFM, on the other hand, consistently shows higher variability in DTW, reflecting greater shape variability across predictions.

Taken together, these results suggest that neither model fully reproduces the variability observed in human motion velocities. The range of variability produced by OPM is more like the observed inter-subject variability measured by RMSE and the range of variability produced by SFM is more like the observed inter-subject variability measured by DTW.

3.3. Upper extremity joint configuration

This section evaluates the performance of the two prediction methods, OPM and SFM, in predicting the seven degrees of freedom (DOFs) of the right arm: shoulder (3 DOFs), elbow (1 DOF), and wrist (3 DOFs). Figure 9 shows the distribution of joint angles for Task 2 across all subjects, comparing experimental data with predictions from OPM and SFM. Each boxplot presents the interquartile range (IQR), median, and distribution of joint angles, allowing for a visual comparison of predicted and observed motion ranges for each DOF for Task 2.

The observed joint angles for the shoulder_z, shoulder_y, and wrist_y exhibit broad distributions, indicating substantial variability in how participants approached the task using those joints. In contrast, shoulder_x and wrist_z exhibit narrower distributions, indicating more narrow use across subjects.

OPM predictions (blue) align well with the experimental data in joints like wrist_y and wrist_x but deviate in others, such as shoulder_y, and elbow_z, overestimating or underestimating, respectively, and shifting the distribution range. SFM predictions (red) show closer alignment in shoulder_x, and wrist_x but underestimate variability in wrist_y and overestimates in elbow_z. Thus, neither prediction method fully captures the general range of joint angles used during the reaching motions in the observed data.

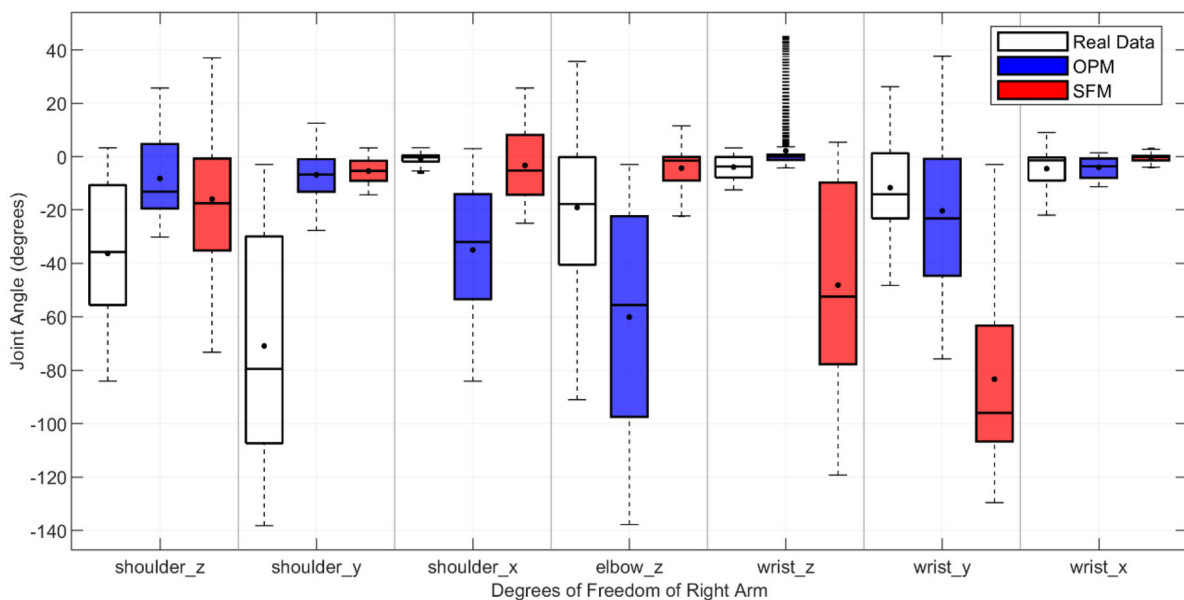


Figure 9. Distribution of joint angle values for Task 2 across the seven DOFs of the right upper extremity, encompassing the shoulder, elbow, and wrist. For each DOF, three boxplots are shown representing the observed data, the OPM predictions, and the SFM predictions. Each box displays the IQR with the black horizontal line indicating the median, and black circles denoting the mean joint angle across all subjects. Whiskers extend to $1.5 \times$ the IQR, and outliers are shown as black ticks.

Table 13. RMSE evaluation per joint (shoulder, elbow, and wrist) across all tasks, comparing OPM and SFM.

	OPM							SFM						
	s_z	s_y	s_x	e_z	w_z	w_y	w_x	s_z	s_y	s_x	e_z	w_z	w_y	w_x
Task 1														
Average of RMSE	14.6	10.9	13.3	39.4	6.8	3.3	1.6	18.1	14.4	22.6	33.7	7.6	4.0	2.1
SD of RMSE	6.7	3.3	6.7	16.5	3.9	2.0	1.4	7.7	6.9	4.2	14.0	3.4	2.4	2.2
Std error of RMSE	2.1	1.1	2.1	5.2	1.2	0.6	0.4	2.4	2.2	1.3	4.4	1.1	0.7	0.7
Task 2														
Average of RMSE	6.2	7.7	10.6	16.1	5.3	2.6	3.9	18.2	16.6	7.8	22.2	5.6	2.6	1.0
SD of RMSE	2.8	3.4	11.7	6.8	3.9	1.0	8.3	8.4	8.0	3.9	8.7	3.7	0.9	0.9
Std error of RMSE	0.9	1.1	3.9	2.3	1.3	0.3	2.8	2.8	2.7	1.3	2.9	1.2	0.3	0.3
Task 3														
Average of RMSE	7.0	2.6	6.1	20.0	6.5	3.8	1.4	6.5	5.3	7.2	15.7	7.3	4.1	1.6
SD of RMSE	4.9	2.1	3.9	11.3	6.3	2.6	1.2	3.2	3.2	4.3	8.3	7.1	2.7	1.3
Std error of RMSE	1.6	0.6	1.2	3.6	2.0	0.8	0.4	1.0	1.0	1.4	2.6	2.2	0.8	0.4
Task 4														
Average of RMSE	24.4	10.2	28.1	35.0	8.8	3.9	3.5	25.5	11.7	36.5	42.5	9.2	4.8	3.6
SD of RMSE	12.3	4.0	14.6	16.8	6.6	2.1	3.5	12.5	7.8	12.1	20.4	6.0	2.4	3.3
Std error of RMSE	4.1	1.3	4.9	5.6	2.2	0.7	1.2	4.2	2.6	4.0	6.8	2.0	0.8	1.1

RMSE is shown in cm/s. Bold values indicate better performance.

Table 14. DTW values across all joint angles for each task.

	Task 1		Task 2		Task 3		Task 4	
	OPM	SFM	OPM	SFM	OPM	SFM	OPM	SFM
Average of DTW	5.0	5.2	3.5	4.4	5.2	5.4	5.9	6.7
SD of DTW	1.5	1.3	1.0	1.4	0.8	1.0	1.0	1.5
Std error of DTW	0.5	0.4	0.3	0.5	0.3	0.3	0.3	0.5

Bold values indicate better performance.

Table 13 presents the RMSE evaluation per joint angle across all four tasks. The elbow_z joint consistently yields the highest RMSE values across all tasks for both methods, particularly in Tasks 1 and 4, with scores reaching up to 39.4° for OPM and 42.5° for SFM, indicating greater difficulty in accurately predicting the elbow joint during the reaching motion. In contrast, the wrist_y and wrist_x joints consistently show the lowest RMSE values, with OPM achieving values as low as 1.4° and SFM as low as 1.0° across tasks.

Although SFM performs better in specific joints for certain tasks, OPM yields a lower average RMSE across all joints and tasks (10.8° vs. 12.8°), suggesting a slightly better prediction of the magnitude of joint configurations.

Table 14 summarizes DTW scores for the full 7-DOF joint angles trajectories. Across all four tasks, OPM consistently achieves lower DTW values than SFM, with the largest differences observed in Task 2 (3.5° for OPM vs. 4.4° for SFM) and Task 4 (5.9° for OPM vs. 6.7° for SFM), indicating that OPM more accurately captures the overall shape of joint coordination patterns.

3.3.1. Modeled inter-subject joint configuration variability

Table 15 presents the RMSE-based inter-subject variability for each joint angle across all tasks. Again, the observed data show the highest variability in nearly all joints and tasks, reflecting differences in individual movement strategies. Between the two models, OPM generally preserves more inter-subject variability than SFM, particularly in the shoulder and elbow joints. However, it occasionally also exhibits its greater variability relative to the observed data.

Table 16 presents DTW measured inter-subject variability for each joint angle across all tasks. The variability of the observed data is the highest across all tasks, and SFM captures closer to the average and range exhibited by the observed data.

Table 15. Inter-subject variability for arm joint angle configuration. RMSE reported as mean \pm SD (Min-Max). Bold indicates the method with an average closer to observed values.

Method	Shoulder _z	Shoulder _y	Shoulder _x	Elbow	Wrist _z	Wrist _y	Wrist _x
RMSE—Task 1							
Real	24.6 \pm 12.3 (7.1–53.0)	13.2 \pm 9.2 (2.7–32.2)	34.9 \pm 17.0 (6.1–72.0)	37.1 \pm 19.8 (10.4–87.4)	16.0 \pm 8.2 (2.3–37.4)	5.5 \pm 2.3 (1.7–12.0)	5.4 \pm 4.8 (1.0–17.6)
OPM	9.1 \pm 4.5 (2.1–20.0)	11.2 \pm 8.6 (1.4–28.4)	24.4 \pm 12.5 (1.5–47.1)	18.5 \pm 11.0 (3.7–43.2)	12.5 \pm 7.8 (0.6–34.0)	4.5 \pm 2.0 (0.8–9.7)	3.9 \pm 3.9 (0.3–13.7)
SFM	12.1 \pm 5.3 (3.9–26.2)	15.5 \pm 8.4 (1.5–35.0)	19.2 \pm 11.1 (1.0–45.8)	18.2 \pm 7.8 (5.3–37.1)	11.2 \pm 7.7 (0.5–33.6)	3.9 \pm 2.0 (0.3–9.3)	2.8 \pm 2.4 (0.3–9.7)
RMSE—Task 2							
Real	14.0 \pm 6.2 (3.2–27.1)	7.8 \pm 2.6 (1.9–13.7)	20.0 \pm 10.2 (2.7–35.7)	17.1 \pm 9.7 (2.8–46.9)	10.2 \pm 4.9 (2.9–25.8)	5.9 \pm 2.6 (1.9–12.3)	2.7 \pm 1.4 (0.4–6.3)
OPM	9.9 \pm 5.5 (0.5–17.8)	6.9 \pm 3.3 (1.7–15.8)	28.7 \pm 18.3 (2.3–69.2)	7.1 \pm 4.4 (0.5–16.4)	9.7 \pm 6.1 (0.4–25.9)	5.3 \pm 2.9 (1.1–10.6)	7.9 \pm 10.7 (0.3–29.5)
SFM	20.6 \pm 11.2 (1.9–43.5)	20.4 \pm 11.0 (4.5–47.3)	23.1 \pm 11.4 (3.7–45.3)	16.2 \pm 10.2 (4.2–40.4)	9.3 \pm 6.2 (0.3–25.1)	4.9 \pm 2.8 (1.1–10.3)	2.0 \pm 1.4 (0.1–5.6)
RMSE—Task 3							
Real	15.7 \pm 7.2 (4.2–37.3)	7.1 \pm 3.3 (1.5–14.9)	35.4 \pm 19.7 (5.0–78.8)	24.2 \pm 15.2 (6.7–58.4)	12.2 \pm 5.2 (2.8–21.6)	4.8 \pm 2.0 (1.9–8.8)	4.1 \pm 2.5 (0.5–11.7)
OPM	13.0 \pm 8.3 (2.8–39.4)	5.9 \pm 3.4 (0.7–14.9)	31.7 \pm 17.7 (4.7–69.8)	19.1 \pm 11.2 (2.7–46.9)	10.3 \pm 5.2 (1.9–23.2)	3.6 \pm 1.6 (0.7–7.0)	3.5 \pm 2.0 (0.3–8.7)
SFM	10.1 \pm 4.9 (1.6–21.5)	7.3 \pm 4.2 (1.5–18.6)	28.9 \pm 16.8 (4.2–70.3)	13.7 \pm 6.9 (3.2–31.0)	10.5 \pm 6.1 (1.3–25.9)	2.7 \pm 1.3 (0.3–6.1)	3.3 \pm 2.0 (0.2–7.3)
RMSE—Task 4							
Real	39.9 \pm 19.7 (6.1–85.4)	14.5 \pm 8.5 (3.4–34.5)	54.8 \pm 27.0 (9.7–117.6)	33.3 \pm 17.0 (8.3–76.2)	16.3 \pm 8.7 (2.9–35.0)	7.8 \pm 3.4 (1.8–13.9)	6.6 \pm 4.3 (0.8–17.0)
OPM	38.0 \pm 22.5 (1.9–89.0)	5.4 \pm 2.7 (0.9–11.6)	42.9 \pm 18.4 (12.3–76.0)	8.3 \pm 4.0 (1.2–18.9)	10.1 \pm 7.8 (0.3–34.0)	5.7 \pm 2.6 (0.9–11.4)	2.2 \pm 1.4 (0.3–5.8)
SFM	34.5 \pm 17.3 (3.0–66.2)	7.8 \pm 3.8 (1.6–15.5)	46.7 \pm 24.3 (12.1–99.4)	12.3 \pm 5.1 (3.6–23.7)	10.2 \pm 8.2 (0.2–35.2)	4.3 \pm 1.9 (0.8–8.0)	2.3 \pm 1.5 (0.4–5.9)

Table 16. Inter-subject variability for upper extremity joint angle configuration.

DTW	Task 1	Task 2	Task 3	Task 4
Real	5.7 \pm 1.3 (2.9–8.6)	4.2 \pm 1.2 (1.5–6.1)	6.4 \pm 1.1 (4.4–9.9)	7.1 \pm 1.4 (3.9–10.0)
OPM	2.9 \pm 2.0 (0.1–8.0)	2.3 \pm 1.1 (0.0–4.9)	3.5 \pm 1.7 (0.1–8.0)	3.7 \pm 2.4 (0.3–10.2)
SFM	5.0 \pm 1.9 (1.6–9.9)	3.9 \pm 1.3 (0.8–6.4)	4.2 \pm 1.6 (1.1–8.9)	4.8 \pm 1.4 (2.5–9.3)

DTW is reported as mean \pm SD (min–max). Bold indicates the method with an average closer to observed values.

Table 17. Summary of the best-performing prediction method for each movement aspect, based on accuracy (RMSE and DTW) and behavioral variability across subjects.

	Accuracy		Modeled inter-subject variability	
	Magnitude (RMSE)	Shape (DTW)	Magnitude (RMSE)	Shape (DTW)
Path	SFM	SFM	SFM	SFM
Velocity	SFM	SFM	OPM	SFM
Upper extremity joint configuration	OPM	OPM	OPM	SFM

4. Discussion

We compared two distinct methods for predicting human reaching motions in 3D space. The comparison focused on three key components of reaching behavior: path, velocity, and arm joint configuration. By evaluating predictions across these motion components, the study aimed to assess both the accuracy and the ability of each method to capture inter-individual variability.

4.1. Results

The evaluation of prediction accuracy and inter-subject variability across the three motion components revealed distinct performance patterns for the two methods (Table 17).

For the path, SFM consistently outperformed OPM in both accuracy and variability. It achieved lower RMSE and DTW values in most tasks and produced subject-to-subject differences in spatial paths that more closely matched those observed in the experimental data. These results indicate that SFM better preserves both the magnitude and shape of individual spatial strategies.

For the velocity, SFM achieved higher accuracy overall. It produced lower DTW values across most tasks and replicated observed peak velocities more closely than OPM. However, OPM better captured inter-subject differences in overall velocity levels, as indicated by RMSE-based inter-subject variability. In contrast, SFM showed lower DTW-based variability, suggesting it better captured the differences in the shape of individual velocity profiles.

For the arm joint configuration, OPM yielded higher prediction accuracy, with lower RMSE and DTW values across tasks. It also better reproduced variability in joint angle magnitude across individuals, while SFM captured more shape variability in the coordination patterns. This suggests that OPM provides more precise joint estimates, whereas SFM reflects more variation in how subjects perform the same task.

These results reflect a general tradeoff between accuracy and diversity representation. Methods that achieve high prediction accuracy often produce more uniform outputs, while those that preserve inter-subject variability may sacrifice precision. Incorporating both RMSE and DTW in the evaluation provides a more complete understanding of these dynamics across motion components.

To synthesize the findings across the three evaluated components: path, velocity, and arm configuration, [Table 17](#) provides a summary of the best-performing method for each evaluated aspect, considering both predictive accuracy and the ability to replicate behavioral variability observed in human data. Accuracy reflects performance based on RMSE and DTW metrics, while behavioral variability refers to how well each method preserves the diversity of individual movement patterns.

4.2. Evaluation metrics: Complementary roles of RMSE and DTW

In this study, RMSE and DTW were utilized together to assess the accuracy and modeled variability of motion predictions across subjects for different components of reaching behavior. RMSE is widely used for quantifying point-wise differences between predicted and observed values. However, RMSE evaluates each time step independently and does not consider the overall structure or timing of the motion, which can lead to misleading conclusions when sequences exhibit differences in spatial or temporal scale and alignment. To address this limitation, DTW was introduced as a complementary metric to compare time-dependent sequences by non-linearly aligning them in time. DTW provides a single value that reflects the best alignment between two multivariate sequences, offering a more holistic view of motion similarity.

DTW has been widely used in fields such as gait recognition (Boulgouris et al., 2004), activity classification (Seto et al., 2015), and trajectory clustering (Zhang et al., 2022), where its ability to align time-series data non-linearly makes it particularly suitable for shape-based comparisons. However, despite its demonstrated strengths, DTW has rarely been adopted as a quantitative evaluation metric for predictive modeling in multivariate human motion contexts. In this study, we extend DTW's use to evaluate how well model-generated multivariate trajectories (path, velocity, joint configuration) replicate collected experimental motions.

Prior work in other domains has demonstrated DTW's robustness across both simulated and real-world data. For example, Cleasby et al. (2019) found DTW and Fréchet distance to be the most responsive metrics when comparing animal trajectories, outperforming commonly used measures for trajectory similarity. Likewise, Laperre et al. (2020) illustrated that DTW can outperform RMSE in evaluating predictions with temporal shifts in the context of geomagnetic storm forecasting, where DTW more effectively captured structural and temporal mismatches between predicted and actual data. Similarly, in time-series classification and motion gesture studies, DTW has shown superior performance due to its sensitivity to sequence shape and flexibility to temporal misalignment (Gloumakov et al., 2020; Jiang et al., 2017; Yu & Xiong, 2019).

Our findings show that RMSE and DTW often lead to different conclusions about model performance depending on what aspect of the motion is being assessed. For instance, as seen in [Tables 6](#) and [9](#),

the best- and worst-predicted subjects per task often differ depending on whether RMSE or DTW is used. This divergence reflects the distinct components of motion each metric captures, highlighting that relying on a single metric can bias or mislead conclusions about critical aspects of model behavior and performance. Understanding not just how many errors exist but also what kind of errors are measured and each model is prone to is essential for meaningful evaluations.

Taken together, our results suggest that combining RMSE and DTW enables a more complete understanding of model behavior by capturing both the local and structural accuracy, as well as the variability, of motion predictions. By applying DTW to full multivariate outputs, this study highlights the metric's potential as a rigorous evaluation metric for multivariate, time-dependent human motion prediction models.

4.3. Differences between prediction methods

The differences in performance between OPM and SFM can be attributed to how each method operates and the type of assumptions embedded in their design. OPM formulates reaching motion as a constrained optimization problem. It uses cubic B-spline curves for joint angles and optimizes a multi-objective cost function combining joint displacement minimization and end-effector velocity maximization. This produces smooth, globally coordinated joint trajectories, resulting in higher accuracy for arm configuration prediction. However, OPM tends to produce uniform trajectories across subjects, which may limit its ability to capture the diversity observed in human movement. In contrast, the SFM combines three rule-based models: an adaptive velocity profile, a dynamic path planner (SDM), and an inverse kinematics solver (FABRIK). These components are applied sequentially but are also interconnected: the velocity profile influences the path planner, which then informs the joint configuration solver, which may adjust the path if the path target is not within the arm's reaching space. This modular and reactive structure allows SFM to better replicate variation in velocity and spatial paths between individuals, resulting in higher shape similarity and modeled variability, particularly for path and velocity.

In addition to the observed performance differences, the two prediction methods differ fundamentally in how movement variability emerges from their underlying structures. The SFM generates motion through a sequence of state-dependent, local control decisions, where variations in initial posture, target geometry, and estimated peak velocity directly influence the evolving path and velocity profiles. Because these components interact dynamically during the simulation, small differences in inputs can lead to distinct movement trajectories, allowing inter-individual variability to be preserved without explicitly modeling subject-specific strategies. In contrast, OPM formulates motion prediction as a global optimization problem, where trajectories are shaped by a shared objective function and a set of local and global constraints, leading to more regularized solutions across subjects.

These structural differences also impose distinct theoretical limits on the two approaches. The optimization-based formulation of OPM inherently biases solutions toward smooth, globally coordinated trajectories and may underrepresent alternative movement strategies when multiple feasible solutions exist. Conversely, the sequential and modular nature of SFM makes the method sensitive to parameter choices and to error propagation across components, as inaccuracies in early stages of path or velocity generation can influence downstream joint configuration estimates. As a result, neither approach is universally optimal; each is constrained by the assumptions embedded in its design and is therefore better suited to different modeling objectives.

An important aspect of the comparison is that the two prediction methods rely on different types and amounts of input information. OPM requires detailed initial posture information and explicit task-level constraints, such as total movement duration, to generate an optimal solution. In contrast, SFM relies on a reduced set of inputs, combined with behavioral cues, such as estimated peak velocity and heading direction, to generate sequentially a feasible motion. This asymmetry reflects inherent differences in the core design of the two approaches.

From a practical perspective, these differing input requirements affect performance consistency across users and scenarios. Methods that depend on richer or more precise inputs may achieve higher

Table 18. Overview of prediction methods and their key characteristics.

	OPM	SFM
Input	Initial spatial position; goal spatial position; total task time; initial arm posture	Initial spatial position; goal spatial position; initial velocity; estimated peak velocity; initial arm posture
Output	7-DOF joint angle trajectories (path, velocity, arm joint configuration)	7-DOF joint angle trajectories (path, velocity, arm joint configuration)
How solution is found	Search into the full solution space to find the optimal solution	Applies rule-based logic to generate a feasible solution sequentially
Pros	+ Allows optimization of multiple objectives	+ Modular and adaptable + Low computational cost
Cons	- Computationally expensive - Requires complete initial data	- May not always reach the target - Dependent on parameter tuning

accuracy when such information is available, but their applicability can be limited in contexts where input data are incomplete, uncertain, or user-dependent. Conversely, methods that operate with fewer or more abstract inputs may offer greater flexibility and accessibility across individuals and use cases, albeit sometimes at the expense of joint-level precision. These tradeoffs should therefore be considered when selecting a prediction method for a given application.

To better illustrate the differences between the two methods, Table 18 provides a side-by-side overview of key characteristics, including input requirements, solution strategy, and performance tradeoffs. The models also differ in the nature and specificity of their inputs. OPM emphasizes temporal constraints and initial joint configuration, while SFM relies more on behavioral cues such as peak velocity and heading direction. These differences influence not only computational demand and implementation complexity, but also the adaptability and generalizability of each method across different use cases. Ultimately, the choice between OPM and SFM depends on the intended application. Tasks that require biomechanical precision, full-body coordination, or high-fidelity posture simulation, such as ergonomic risk assessment, may benefit more from OPM. In contrast, the flexibility and efficiency of SFM may better serve tasks emphasizing behavioral variability, real-time interaction, or adaptive simulation in human-computer interaction, where capturing the variability and path dynamics support adaptive behavior in computer-controlled systems.

4.4. Limitations

While the study provides valuable insights, several limitations must be acknowledged. First, the parameters of the SDM and velocity models within the SFM were manually selected through iterative testing based on observed prediction behavior. No automated parameter optimization or formal sensitivity analysis was performed, which may limit objectivity and generalizability across tasks or populations. At the same time, this manual parameterization should be seen as a conservative assessment of the SFM, since suboptimal parameter choices are more likely to decrease predictive performance than artificially enhance it. Future work will therefore focus on systematic parameter estimation and optimization to improve the robustness and generalizability of the proposed framework.

Second, the experimental tasks were performed without physically defined start or end points. Instead, participants were instructed verbally to perform movements as if seated in a vehicle. This open-ended task design may have led to inconsistencies in how participants interpreted and executed the movements, particularly regarding initial posture and endpoint location, which could have contributed to larger prediction errors in certain tasks and made some components of the motion more difficult to model accurately.

Third, the study involved a limited sample of ten participants performing four distinct reaching tasks. While this was sufficient to support the methodological comparison and identify key differences between the models, the scope of the dataset constrains broader generalization. Future studies incorporating a larger and more diverse participant pool and a wider range of reaching scenarios could provide deeper insight into model performance across contexts.

4.5. Model improvements and future work

The comparative evaluation of OPM and SFM highlights clear areas where each method can be refined to improve overall prediction quality. For OPM, refining the cost function, particularly to better capture motion shape, could enhance shape similarity and improve the model's ability to reflect inter-subject differences. This adjustment may lead to more realistic trajectory predictions while maintaining joint accuracy. For SFM, improvements may be achieved by systematically tuning the SDM parameters to reduce spatial magnitude errors and improve alignment with observed joint configurations. In addition, incorporating a more rigorous definition of joint or posture-related constraints within the FABRIK module could improve the plausibility and accuracy of predicted arm configurations.

In addition to refining each model, future work could expand by including a broader set of reaching tasks. Tasks involving obstacle avoidance or continuous movement within constrained environments may offer further insights into model behavior and expose limitations that were not evident in the current set of tasks. Lastly, the findings of this study emphasize the importance of using multiple evaluation metrics when assessing predictive performance in human motion modeling. Further work to gain a clearer understanding of what each metric captures and what it may fail to represent is essential for improving both model evaluation and future model development, particularly when aiming to reproduce the complexity and richness of human movement.

5. Conclusion

This study presents a novel prediction model, the SFM, and an initial evaluation of its performance relative to an established prediction model, the OPM. While the results were mixed, each model demonstrated distinct strengths and weaknesses.

The use of DTW, alongside RMSE, enables a more comprehensive and nuanced evaluation of the models, revealing differences in both how closely the predicted motions match the observed data and how well they preserve the temporal structure and coordination patterns of natural human movement. This dual-metric approach proves value in identifying tradeoffs between predictive accuracy and the ability to replicate inter-subject variation, an aspect often overlooked in conventional evaluations, which typically evaluate accuracy using only RMSE.

The results showed that SFM consistently achieved higher accuracy and better replication of inter-subject variability for spatial paths, with lower RMSE and DTW values across most tasks. Similarly, SFM outperformed OPM in velocity prediction by more closely matching observed peak velocities and better capturing the shape of individual velocity profiles, as reflected by lower DTW values. In contrast, OPM yielded higher accuracy for upper extremity joint configurations, achieving lower RMSE and DTW values and more precise reproduction of joint angle magnitudes across subjects. These findings indicate a clear tradeoff between predictive precision and the ability to represent behavioral diversity. OPM favors biomechanical accuracy and smooth, globally coordinated joint trajectories, whereas SFM better preserves individual differences in spatial and temporal movement patterns, particularly for path and velocity components.

The distinct model structures, input requirements, and computational characteristics help explain these differences and highlight the importance of aligning model selection with application-specific priorities. Ultimately, the choice between OPM and SFM depends on the intended use case and the type of data available. Applications requiring high-fidelity joint-level accuracy, such as detailed ergonomic or biomechanical analyses, may benefit more from OPM, whereas applications emphasizing behavioral variability, adaptability, or interactive simulation may be better served by SFM. Though this assessment is likely to change as both approaches are improved and validated over time.

Overall, this evidence-based comparison demonstrates that SFM constitutes a promising complementary approach to existing optimization-based methods for human motion prediction, while also highlighting the need for further development and validation to improve its robustness and generalizability.

Author contributions

CRedit: **Estela Pérez Luque**: Conceptualization, Formal analysis, Methodology, Writing – original draft, Writing – review & editing; **Seunghun Lee**: Formal analysis, Methodology, Writing – review & editing; **Dan Högberg**: Funding acquisition, Supervision, Writing – review & editing; **James Yang**: Funding acquisition, Methodology, Supervision, Writing – review & editing; **Maurice Lamb**: Conceptualization, Methodology, Supervision, Writing – review & editing.

Disclosure statement

No potential competing interest was reported by the authors.

Funding

This work has been made possible with support from the Swedish Knowledge Foundation through projects entitled IGP-HENCE (20200184) and ADOPTIVE (20200003). This support is gratefully acknowledged.

ORCID

Estela Pérez Luque  <http://orcid.org/0000-0003-0746-9816>
 Seunghun Lee  <http://orcid.org/0009-0000-6152-7250>
 Dan Högberg  <http://orcid.org/0000-0003-4596-3815>
 James Yang  <http://orcid.org/0000-0003-0842-7933>
 Maurice Lamb  <http://orcid.org/0000-0003-2254-1396>

References

- Corcus, D. M., Gottlieb, G. L., & Agarwal, G. C. (1989). Organizing principles for single-joint movements. II. A speed-sensitive strategy. *Journal of Neurophysiology*, 62(2), 358–368. <https://doi.org/10.1152/jn.1989.62.2.358>
- Aristidou, A., & Lasenby, J. (2011). FABRIK: A fast, iterative solver for the Inverse Kinematics problem. *Graphical Models*, 73(5), 243–260. <https://doi.org/10.1016/j.gmod.2011.05.003>
- Aristidou, A., Chrysanthou, Y., & Lasenby, J. (2016). Extending FABRIK with model constraints. *Computer Animation and Virtual Worlds*, 27(1), 35–57. <https://doi.org/10.1002/cav.1630>
- Boulgouris, N. V., Plataniotis, K., & Hatzinakos, D. (2004). Gait recognition using dynamic time warping. In *IEEE 6th Workshop on Multimedia Signal Processing (MMSP), Siena, Italy* (pp. 263–266).
- Braun, C., Ortiz-Haro, J., Toussaint, M., & Oguz, O. (2021). RHH-LGP: Receding horizon and heuristics-based logic-geometric programming for task and motion planning.
- Cao, C., Yang, C., Zhang, R., & Liu, S. (2023). Discovering intrinsic spatial-temporal logic rules to explain human actions.
- Clark, R., Dickinson, T., Loaiza, J., Geiger, D. W., & Charles, S. K. (2020). Tracking joint angles during whole-arm movements using electromagnetic sensors. *Journal of Biomechanical Engineering*, 142(7), 074502. <https://doi.org/10.1115/1.4045814>
- Cleasby, I. R., Wakefield, E. D., Morrissey, B. J., Bodey, T. W., Votier, S. C., Bearhop, S., & Hamer, K. C. (2019). Using time-series similarity measures to compare animal movement trajectories in ecology. *Behavioral Ecology and Sociobiology*, 73(11), 151. <https://doi.org/10.1007/s00265-019-2761-1>
- Cloutier, A., Boothby, R., & Yang, J. (2011). 6777 LNCS:59 – Motion capture experiments for validating optimization-based human models. In *Lecture notes in computer science (including subseries lecture notes in artificial intelligence and lecture notes in bioinformatics)* (p. 68).
- Cui, Q., Sun, H., & Yang, F. (2020). Learning dynamic relationships for 3D human motion prediction. In *Proceedings of the IEEE computer society conference on computer vision and pattern recognition* (pp. 6518–6526).
- Demirel, H. O., Ahmed, S., & Duffy, V. G. (2022). Digital human modeling: A review and reappraisal of origins, present, and expected future methods for representing humans computationally. *International Journal of Human-Computer Interaction*, 38(10), 897–937. <https://doi.org/10.1080/10447318.2021.1976507>
- Denavit, J., & Hartenberg, R. S. (1955). A kinematic notation for lower-pair mechanisms based on matrices. *Journal of Applied Mechanics*, 22(2), 215–221. <https://doi.org/10.1115/1.4011045>
- Fajen, B. R., & Warren, W. H. (2007). Behavioral dynamics of intercepting a moving target. *Experimental Brain Research*, 180(2), 303–319. <https://doi.org/10.1007/s00221-007-0859-6>
- Fajen, B., & Warren, W. (2003). Behavioral dynamics of steering, obstacle avoidance, and route selection. *Journal of Experimental Psychology. Human Perception and Performance*, 29(2), 343–362. <https://doi.org/10.1037/0096-1523.29.2.343>

- Farahani, S. D., Bertucci, W., Andersen, M. S., Zee, M. d., & Rasmussen, J. (2015). Prediction of crank torque and pedal angle profiles during pedaling movements by biomechanical optimization. *Structural and Multidisciplinary Optimization*, 51(1), 251–266. <https://doi.org/10.1007/s00158-014-1135-6>
- Fitts, P. M. (1954). The information capacity of the human motor system in controlling the amplitude of movement. *Journal of Experimental Psychology*, 47(6), 381–391. <https://doi.org/10.1037/h0055392>
- Furuki, D., & Takiyama, K. (2017). Detecting the relevance to performance of whole-body movements. *Scientific Reports*, 7(1), 15659. <https://doi.org/10.1038/s41598-017-15888-3>
- Gang, C., & Wang, Y. (2025). Human motion prediction, reconstruction, and generation. arXiv. <http://arxiv.org/abs/2502.15956>.
- Gibson, J. J. (1979). *The ecological approach to visual perception*. Houghton Mifflin.
- Gloumakov, Y., Spiers, A. J., & Dollar, A. M. (2020). Dimensionality reduction and motion clustering during activities of daily living: 3, 4, and 7 degree-of-freedom arm movements. arXiv. <http://arxiv.org/abs/2003.02641>
- Gong, W., Xie, X., & Liu, Y.-J. (2018). Human experience-inspired path planning for robots. *International Journal of Advanced Robotic Systems*, 15(1), 1729881418757046. <https://doi.org/10.1177/1729881418757046>
- Gottlieb, G. L., Corcos, D. M., & Agarwal, G. C. (1989). Organizing principles for single-joint movements. I. A speed-insensitive strategy. *Journal of Neurophysiology*, 62(2), 342–357. <https://doi.org/10.1152/jn.1989.62.2.342>
- Hamm, K. (2020). Time, velocity, and speed.
- Harrison, H. S., Turvey, M. T., & Frank, T. D. (2016). Affordance-based perception-action dynamics: A model of visually guided braking. *Psychological Review*, 123(3), 305–323. <https://doi.org/10.1037/rev0000029>
- Huaining, C., Louise, O., & Annette, R. (1994). *Generator of body data (GEBOD) manual*. Wright-Patterson AFB.
- Jiang, J., Xing, Y., Wang, S., & Liang, K. (2017). Evaluation of robotic surgery skills using dynamic time warping. *Computer Methods and Programs in Biomedicine*, 152(1), 71–83. <https://doi.org/10.1016/j.cmpb.2017.09.007>
- Kim, S., Nozaki, T., & Murakami, T. (2016). An approach to categorization analysis for human motion by Kinect and IMU. In *IECON proceedings (industrial electronics conference)* (pp. 6158–6162).
- Klein, H., Jaquier, N., Meixner, A., & Asfour, T. (2022). A Riemannian take on human motion analysis and re-targeting. In *2022 IEEE/RSJ international conference on intelligent robots and systems (IROS), Kyoto, Japan, IEEE* (pp. 5210–5217). <https://ieeexplore.ieee.org/document/9982127/>. <https://doi.org/10.1109/IROS47612.2022.9982127>
- Lamb, M., Kallen, R. W., Harrison, S. J., Di Bernardo, M., Minai, A., & Richardson, M. J. (2017). To pass or not to pass: Modeling the movement and affordance dynamics of a pick and place task. *Frontiers in Psychology*, 8, 1061. <https://doi.org/10.3389/fpsyg.2017.01061>
- Lamb, M., Lee, S., Billing, E., Högberg, D., & Yang, J. (2022). Forward and Backward Reaching Inverse Kinematics (FABRIK) solver for DHM: A pilot study. In *Proceedings of the 7th international digital human modeling symposium*.
- Laperre, B., Amaya, J., & Lapenta, G. (2020). Dynamic time warping as a new evaluation for DST forecast with machine learning. *Frontiers in Astronomy and Space Sciences*, 7, 39. <https://doi.org/10.3389/fspas.2020.00039>
- Latash, M. L. (2010). Motor synergies and the equilibrium-point hypothesis. *Motor Control*, 14(3), 294–322. <https://doi.org/10.1123/mcj.14.3.294>
- Moreno, L. A. O., & Alcántara, J. H. A. (2022). An adaptation of FABRIK algorithm for serial robot's inverse kinematics. In *2022 IEEE international conference on engineering veracruz (ICEV)* (pp. 1–6). <https://ieeexplore.ieee.org/abstract/document/9959663>. <https://doi.org/10.1109/ICEV56253.2022.9959663>
- Nalepka, P., Lamb, M., Kallen, R. W., Shockley, K., Chemero, A., Saltzman, E., & Richardson, M. J. (2019). Human social motor solutions for human-machine interaction in dynamical task contexts. *Proceedings of the National Academy of Sciences of the United States of America*, 116(4), 1437–1446. <https://doi.org/10.1073/pnas.1813164116>
- Perez Luque, E., Brolin, E., Högberg, D., & Lamb, M. (2022). Challenges for the consideration of ergonomics in product development in the Swedish automotive industry – An interview study. *Proceedings of the Design Society*, 2, 2165–2174. <https://doi.org/10.1017/pds.2022.219>
- Porzio, A. D., & Coraggio, M. (2025). A personalized data-driven generative model of human motion. arXiv. <http://arxiv.org/abs/2503.15225>.
- Rudenko, A., Palmieri, L., Herman, M., Kitani, K. M., Gavrila, D., & Arras, K. (2020). Human motion trajectory prediction: A survey. *International Journal of Robotics Research*, 39(8), 895–935. <https://doi.org/10.1177/0278364920917446>
- Santos, M. C., Molina, L., Carvalho, E. A. N., Freire, E. O., Carvalho, J. G. N., & Santos, P. C. (2021). FABRIK-R: An extension developed based on FABRIK for robotics manipulators. *IEEE Access*, 9, 53423–53435. <https://doi.org/10.1109/ACCESS.2021.3070693>
- Senin, P. (2008). *Dynamic time warping algorithm review*. Information and computer science department. University of Hawaii at Manoa.
- Sethi, A., Stergiou, N., Patterson, T. S., Patten, C., & Richards, L. G. (2017). Speed and rhythm affect temporal structure of variability in reaching poststroke: A pilot study. *Journal of Motor Behavior*, 49(1), 35–45. <https://doi.org/10.1080/00222895.2016.1219304>

- Seto, S., Zhang, W., & Zhou, Y. (2015). Multivariate time series classification using dynamic time warping template selection for human activity recognition. arXiv. <http://arxiv.org/abs/1512.06747>
- Tavenard, R. (2021). An introduction to dynamic time warping. <https://rtavenar.github.io/blog/dtw.html>
- Wang, B., Adeli, E., Chiu, H., & Niebles, J. (2019). Imitation learning for human pose prediction. arXiv. <http://arxiv.org/abs/1909.03449>
- Wilhelms, J., & Gelder, A. (2001). Fast and easy reach-cone joint limits. *Journal of Graphics Tools*, 6(2), 27–41. <https://doi.org/10.1080/10867651.2001.10487539>
- Wolf, A., Miehl, J., & Wartzack, S. (2020). Challenges in interaction modelling with digital human models – A systematic literature review of interaction modelling approaches. *Ergonomics*, 63(11), 1442–1458. <https://doi.org/10.1080/00140139.2020.1786606>
- Xia, X., Zhou, T., Du, J., & Li, N. (2022). Human motion prediction for intelligent construction: A review. *Automation in Construction*, 142, 104497. <https://doi.org/10.1016/j.autcon.2022.104497>
- Xiang, Y., Chung, H.-J., Kim, J. H., Bhatt, R., Rahmatalla, S., Yang, J., Marler, T., Arora, J. S., & Abdel-Malek, K. (2010). Predictive dynamics: An optimization-based novel approach for human motion simulation. *Structural and Multidisciplinary Optimization*, 41(3), 465–479. <https://doi.org/10.1007/s00158-009-0423-z>
- Yang, J., Marler, R. T., Kim, H., Arora, J., & Abdel-Malek, K. (2004). Multi-objective optimization for upper body posture prediction. In *10th AIAA/ISSMO multidisciplinary analysis and optimization conference* (pp. 2288–2305). <https://doi.org/10.2514/6.2004-4506>
- Yang, J., Marler, T., & Rahmatalla, S. (2011). Multi-objective optimization-based method for kinematic posture prediction: Development and validation. *Robotica*, 29(2), 245–253. <https://doi.org/10.1017/S026357471000010X>
- Yu, X., & Xiong, S. (2019). A dynamic time warping based algorithm to evaluate Kinect-enabled home-based physical rehabilitation exercises for older people. *Sensors*, 19(13), 2882. <https://doi.org/10.3390/s19132882>
- Zaman, R., Xiang, Y., Cruz, J., & Yang, J. (2021). Three-dimensional asymmetric maximum weight lifting prediction considering dynamic joint strength. *Proceedings of the Institution of Mechanical Engineers, Part H: Journal of Engineering in Medicine*, 235(4):437–446. <https://doi.org/10.1177/0954411920987035>
- Zhang, K., Lin, S., Sun, H., Ma, L., & Xu, J. (2022). Dynamic time warping based clustering for time series analysis. In *IoT and big data technologies for health care* (pp. 376–385). Springer. https://doi.org/10.1007/978-3-030-94182-6_29

About the authors

Estela Pérez Luque received her doctorate in Informatics from the University of Skövde. Her research focuses on digital human modeling, simulation, and prediction of human posture and motion, with applications in ergonomics and safety, human–computer interaction, and product development.

Seunghun Lee received his doctorate in Mechanical Engineering from Texas Tech University. His research focuses on human body dynamics, motion prediction, and optimization methods for human movement analysis.

Dan Högberg is Professor at the University of Skövde. His research focuses on digital human modeling and methods for integrating ergonomics and human factors knowledge into product development processes to support designers and engineers in virtual design stages.

James Yang is Professor and Director of the Human-Centric Design Research Lab at Texas Tech University. His research interests include digital human modeling, human digital twins, biomechanics, fatigue modeling, healthcare engineering, and driver behavior modeling for autonomous vehicles.

Maurice Lamb is a Senior Lecturer at the University of Skövde. His interdisciplinary research combines cognitive science, philosophy, engineering, and computer science, and focuses on applying complex dynamical systems methods to solve challenges in human–robot and human–agent interaction contexts.